Available online at www.sciencedirect.com

jmr&t Journal of Materials Research and Technology

journal homepage: www.elsevier.com/locate/jmrt

Original Article

Evaluation of structural performances of metakaolin based geopolymer concrete

Fatheali A. Shilar [a], *Sharanabasava V. Ganachari* [b,*], *Veerabhadragouda B. Patil* [c], *Kottakkaran Sooppy Nisar* [d,*]

[a] *Department of Civil Engineering, Jain College of Engineering, Belagavi 590014, INDIA*
[b] *Department of Chemistry, School of Advanced Sciences, KLE Technological University, Hubballi 580031, INDIA*
[c] *Institute of Energetic Materials, Faculty of Chemical Technology, University of Pardubice, Pardubice, CZECH REPUBLIC*
[d] *Department of Mathematics, College of Arts and Sciences, Prince Sattam Bin Abdulaziz University, Wadi Aldawaser 11991, SAUDI ARABIA*

ARTICLE INFO

Article history:
Received 30 May 2022
Accepted 4 August 2022
Available online 28 August 2022

Keywords:
Compressive strength
Temperature
Alkaline to binder ratio
Metakaolin
Potassium

ABSTRACT

Last few decades, there has been a substantial advancement of geopolymer (GP) as a Portland cement substitute. It is vital to investigate potential building uses for geopolymer concrete (GPC). Six different mixes were cast for an alkaline to binder (A/B) ratio of 0.25 –0.50 with an interval of 0.05. Metakaolin-based geopolymer were cured at ambient temperature and tested for 7, 14, 28, and 90 days. Metakaolin-Marble (MM00) mix was observed to have a maximum slump. For an A/B ratio of 0.35, maximum compressive, split tensile, flexural strength and modulus of elasticity was achieved. For elevated temperature resistance, geopolymer concrete cubes were exposed to temperatures (T) of 200, 400, to 600 C. As the temperature increased, compressive strength (CS) reduced. As the increase of the alkaline to binder (A/B) ratio, the strength of geopolymer concrete increases up to a specific limit beyond the limit strength decline. An empirical formula for split tensile (STS) value prediction using compressive strength values is proposed, valid for determining split tensile strength value. The correlation between compressive strength, split tensile strength, flexural strength, and bulk density varies linearly for a quadratic polynomial.
© 2022 The Author(s). Published by Elsevier B.V. This is an open access article under the CC BY-NC-ND license (http://creativecommons.org/licenses/by-nc-nd/4.0/).

1. Introduction

With the rising demand for shelter needs to the growing population, infrastructural expansion, and industrialization globally, there is a need for innovative construction technology and alternative materials to meet these requirements [1]. Sustainability and environment are two significant issues that must be addressed while researching alternative construction materials [2]. In this context, geopolymer concrete (GPC) has emerged as a trending and unexplored area for researchers [3]. GPC has several advantages over standard Portland concrete,

* Corresponding authors.
E-mail addresses: sharanu14@gmail.com (S.V. Ganachari), ksnisar1@gmail.com (K.S. Nisar).
https://doi.org/10.1016/j.jmrt.2022.08.020
2238-7854/© 2022 The Author(s). Published by Elsevier B.V. This is an open access article under the CC BY-NC-ND license (http://creativecommons.org/licenses/by-nc-nd/4.0/).

including decreased carbon emissions, cheaper manu-facturing amount, potential to use waste materials as binders [4].

The geopolymerization reaction mechanism of alumino-silicate dissolution in the activator solution from a chemical perspective (Fig. 1). Resource materials and an alkaline activation solution are the two most essential criteria for geopolymer (GP). The chemical composition of resource materials must contain alumina-silicate, and these materials come from waste by-products like Ground granulated blast-furnaces slag (GGBS), fly ash (FA), and red mud (RM) [6]. According to prior research, the fineness of binders, the chemical composition of binders and activator, the activator agent to binder ratio, molar concentration, curing method, and temperature are some of the factors which enhance the rate of geopolymerization [7,8] shown in Fig. 1.

The SiO_2/Al_2O_3 ratio denotes the proportion of silica SiO_2 to alumina Al_2O_3. The geopolymer compressive strength (CS) is improved when this ratio is increased. The SiO_2/Al_2O_3 ratio constraints the application domains [9]. The SiO_2/Al_2O_3 ratio was employed to categorize different GP applications. As per a past literature study, a substantial intensification in ~~Si/Al~~ SiO_2/Al_2O_3 observed that setting time and the CS were decreased [10,11]. The surface area of the binder is more, which tends to accelerate the rate of the geopolymerization process, causing enhancement of mechanical performances [12,13].

Many earlier experiments have shown that increasing the concentration of the activator agent increases CS up to a certain point, beyond which the CS drops [14]. Past literature study is the only parameter for selecting the molar of the activator. Several investigations have demonstrated that curing temperatures of 12 M NaOH and 60 °C and 70 °C tend to produce the optimum CS results. However, the research suggested using 13 M NaOH for excellent workability. As per past literature, 14 M NaOH has more excellent CS in concrete, whereas 16 M NaOH has the best CS for geopolymer mortar [15–17].

Numerous investigations have established the maximum activator/binder ratio for many precursors [18]. According to literature research, the A/B ratio for GGBS and red-based geopolymer should be between 0.40 and 0.55 [16]. According to the study, for marble-based GPC, a water to binder (W/B) ratio of 0.36 is better suited for achieving maximum CS. According to research, a W/B ratio of 0.30–0.40 is best for producing FA-based GPC. When adding a filler material to FA-based GPC, W/B ratios in the range between 0.35 and 0.55 is the most suggested [15,17]. Enhanced mechanical properties of GPC are achieved by increasing heat curing and its duration until a specified value is obtained [9,18,19]. However, high temperatures induce fractures in the geopolymer binder; for GPC specimens, exposure to a long time for high curing temperature results in a detrimental impact on mechanical strength [20,21]. The optimum CS is attained with a 60–75 °C as curing temperature, for a curing period of 5–7 days, for FA-based GPC, and 1–4 days for GGBS-based GPC [22,23].

The calcination of kaolinite produces MK, a highly reactive pozzolana (China clay). It must be processed in a burning process similar to cement, albeit the manufacturing temperature is between 700 and 900 °C rather than 1450 °C [27,28]. MK is a dehydroxylated version of kaolinite, a clay mineral. MK is clay that is often used in the manufacture of ceramics and utilized as a cement substitute preparation of traditional concrete [25]. Compared to Portland cement, MK has a lower particle size (1–2 μm) and a higher surface area but a bigger particle size than silica fume [26]. MK reacts fast and decreases the diffusion coefficient compared to regular Portland cement because of its tiny particle size and large surface area [27]. The chemical composition of a marble powder majority consists of CaO, which helps develop better strength and helps achieve lower permeability [28,29].

In general, waste generation at many phases of mining and processing activities has contributed to severe environmental concerns in the dimensional stone marble business [30] (see

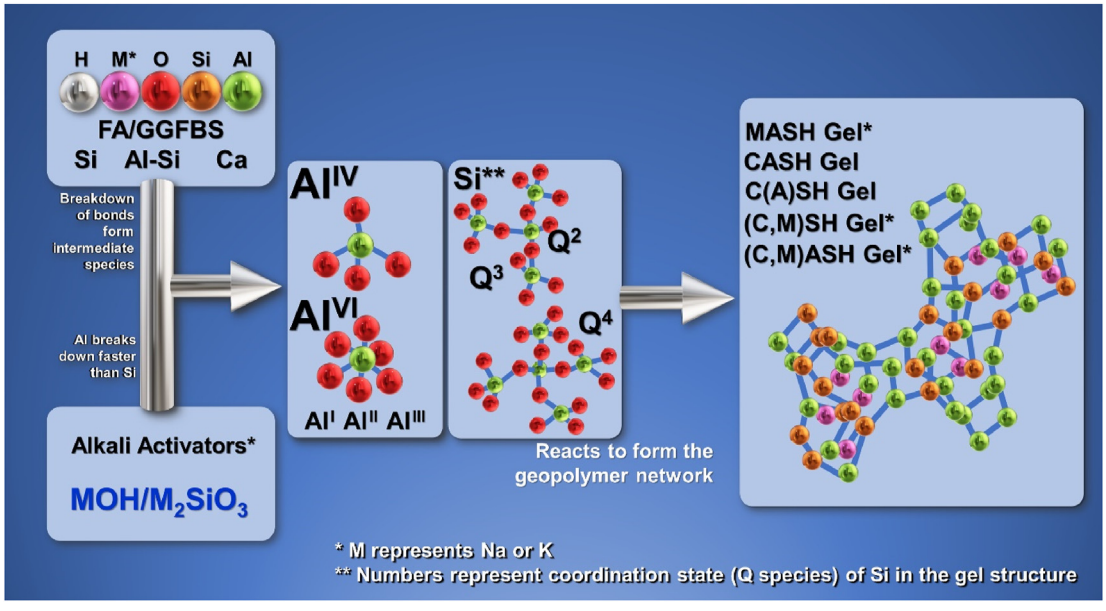

Fig. 1 – Schematic representation of geopolymerization process in GPC [recreated from Ref [5]].

Fig. 2). The sludge produced between 20% and 30% of the weight of the stone processed, depending on the type of procedure used. Marble dust as a binder and sand substitute was studied on mechanical and durability properties. Most of the studies have had favorable results [31]. This application may be utilized to minimize the cost of GPC manufacturing by using waste marble dust as an additive ingredient, affecting mortar mechanical performance [32]. 10% sand replacement with marble in the presence of additives yielded a maximum CS equivalent to the reference combination for 28 days [33].

This research aims to use marble as a binder with MK in the production of GPC. For the optimum percentage of marble content, the fresh and mechanical performances of MK based GPC were investigated in this article. The different proportions of A/B ranging from 0.30, 0.40 and 0.50, were also investigated for testing days of 7, 14, 28 and 90. An empirical formula is proposed for STS value prediction using CS values which were valid for the determination of STS value.

2. Materials and method

2.1. Materials

The marble powder was procured from the Belagavi, Karnataka, in this study. Table 1 shows the chemical composition used in marble and metakaolin (MK). Fig. 1 Production stages of marble. The MK was collected from Mayuri Nagar, Miyapur, Kachiguda, Hyderabad, and Telangana. MK is produced by calcination of kaolin at high temperature. River sand was used for our work. The sand was procured from Mundari and confirmed to IS 383 with specific gravity as 2.4 and fineness modulus as 2.6. Coarse aggregate was procured from Belagavi and confirmed to IS 383 with specific gravity as 2.65 and fineness modulus as 6. Alkaline agents such as potassium silicate (K_2SiO_3) and potassium hydroxide (KOH) were procured from the Shree chemical from Belagavi. K_2SiO_3 and KOH were in pellet form. These pellets were converted in liquid of required concentration by adding water to these pellets. The activator was prepared with a 14 M concentration. After combining the two solutions, they were left to remain for 24 h before being used to finish the interaction. Fig. 3 represents the various ingredients of GPC. Table 2 Represents the physical properties of ingredients of GPC.

2.2. Mixing, casting, and curing

The tested ingredients properties of GPC are shown in Fig. 4 in which MM refers to the mixture marble/MK. In the current study, six different MM mix proportions partially replacing marble by MK (Table 3). A/B was used to prepare GPC as 0.25, to 0.50, with an interval of 0.05. As an activating agent, KOH concentration was kept at 14 M and cured at 50 °C for 7, 14, 28, and 90 days. The Marble and MK as binders were carefully mixed manually until a homogeneous mixture was obtained. Activators were poured into the binders, and the mixtures were mixed using the concrete mixer. Binder and aggregates were dry mixed, and then the activators were poured into the mix. The mold's inner surface was applied with grease, and a three-layer paste of GPC was poured into them. Cubes were compacted using a table vibrator. The total mixing time was 20 min. Cubes were heated at 50 C for 1 h in the oven after 24 h of the final set of cubes, cooled at room temperature, and taken for testing at respectively days (see Table 4)

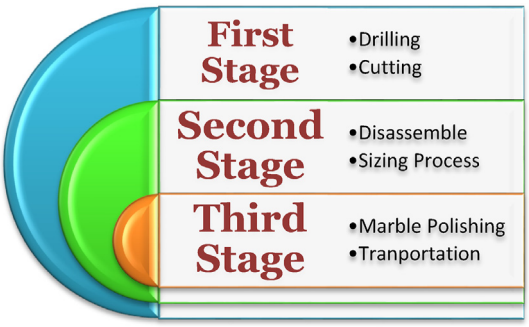

Fig. 2 – Schematic of production stages of marble.

3. Experimental tests

The workability of GPC was carried out as per IS 1199 [34]. Workability such as slump (SV), compaction factor (CF), and vee-bee consistometer (VBC) for a different proportion of marble waste along with various A/B ratios was carried out and results are shown in Fig. 5a–c. The assembly consists of a cone frustum and a tamping rod that has been certified to IS 1199 [38]. The inner surface of the slump cone was cleaned thoroughly. GPC was filled in the four layers. After each layer of GPC was poured into a cone, it was tamped for 25 strokes applied using a tamping rod. After filling GPC in the cone, surface was levelled using a trowel, and the final height of the slump was measured. The SV value is the difference between the two heights, i.e., final and initial (mm).

3.1. Slump

For different ratios of A/B values ranging from 0.25 to 0.50, an interval of 0.05, GPC matrix was prepared. SV value observed after experimentation ranging from 61 (minimum) to 89 mm (maximum) refers to Fig. 5a. For the A/B ratio 0.25, SV range from 61 to 76 mm as the minimum and maximum values. The MM00 shown maximum slump, as 76 mm, and MM25 minimum mix slump was observed as 61 mm. For an A/B ratio of 0.30, the SV range from 68 to 79 mm as the minimum and

Table 1 – Chemical composition of Metakaolin and Marble.

Composition Binder	SiO_2	Al_2O_3	CaO	MgO	K_2O	Fe_2O_3	Na_2O	SO_3	$CaCO_3$	LOI
Metakaolin	55.7	38.6	0.39	2.08	2.43	2.03	0.26	1.1	–	1.74
Marble	1.28	1.38	50.10	1.72	–	0.54	0.29	0.21	44.1	0.39

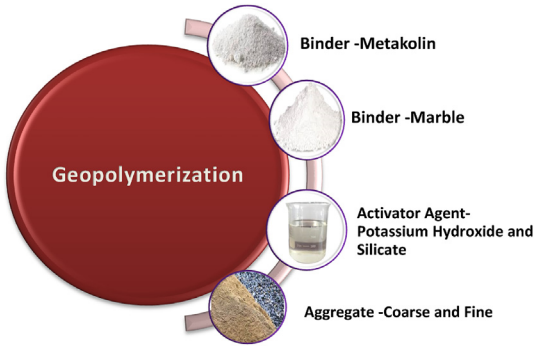

Fig. 3 – Schematic representation of ingredients of GPC.

maximum values, respectively. For MM00 was shown maximum SV, as 79 mm, and MM25 mix minimum SV was observed as 68 mm. For the A/B ratio of 0.35, the SV value was seen from 70 to 82 mm as the minimum and maximum values. The MM00 shown maximum SV, as 82 mm, and MM25 mix minimum SV was observed as 82 mm. For the A/B ratio of 0.40, the SV range from 75 to 85 mm as the minimum and maximum values. The MM00 shown maximum SV as 75 mm, and MM25 mix minimum SV was observed as 85 mm. For the A/B ratio of 0.45, the SV range from 79 to 89 mm as the minimum and maximum values. The MM00 shown maximum SV, as 79 mm, and MM25 mix minimum SV was observed as 89 mm. For an A/B ratio of 0.50, the SV range from 77 to 86 mm as the minimum and maximum values. The MM00 shown maximum SV, as 77 mm, and MM25 mix minimum SV was observed as 86 mm.

3.1.1. *V–B consistometer (VBC)*

For different ratios of A/B values ranging from 0.25 to 0.50, an interval of 0.05 GPC matrix was prepared, as shown in Fig. 5b. VBC value observed after experimentation ranging from 8 s (minimum) to 24 s (maximum) for an A/B ratio of 0.25–0.50. For the A/B ratio of 0.45, maximum VB-time was observed, compared with ratios and mixes. VBC value was observed from 15 to 24 s as the minimum and maximum values. The MM00 shown maximum VBC was observed as 24 s, and MM25 mix minimum VBC was observed as 15 s. As the marble content increased, VB time also increased to the specific limit, and time was reduced beyond that point. Marble content up to optimum usage of 20%, maximum VB time was seen. For an A/B ratio of 0.45, the MM00 mix proportion has the longest VB time compared to other mixes. For an A/B ratio of 0.45, MM00 has a 37% VB time higher than MM25, indicating that MM00 is 37% more workable than MM25. Similarly MM00 has a 8.33%, 16.6%, 25%, and 29.1%, VB time higher than MM05, MM10, MM15, and MM20 respectively.

Table 2 – Physical properties of ingredients of GPC.

Materials	Metakaolin	Marble	Aggregate	R.Sand
Physical Properties				
Specific gravity	2.60	2.55	2.65	2.6
Zone	–	–	–	II
Fineness modulus	–	–	7.0	3.0
Silt content	–	–	–	4%

3.1.2. *Compaction factor (CF)*

For different ratios of A/B values ranging from 0.25 to 0.50, an interval of 0.05, GPC matrix was prepared, refer to Fig. 5c. For the A/B ratio of 0.25, the CF value was observed from 0.68 to 0.75 as the minimum and maximum values. When comparing ratios and mixtures, the highest CF was found for the A/B ratio of 0.45. The lowest and highest CF values are 0.82 and 0.86, respectively. The MM00 mix had the highest maximum CF of 0.86, whereas the MM25 mix have the lowest minimum CF of 0.77. CF increased to the specific limit as the marble content increased, and CF was reduced beyond that point. Maximum CF was observed with marble content up to optimal utilization of 20%. Compared to other mixes, the MM00 mix percentage has the highest CF for an A/B ratio of 0.45. MM00 has a 4.6% greater CF than MM25 for an A/B ratio of 0.45, implying that MM00 is 2.3% more feasible than MM25. MM00 has a CF of 2.3%, 2.33%, 1.1%, and 1.16%, respectively, greater than MM05, MM10, MM15, and MM20.

3.1.3. *Effect of activators on the workability of GPC*

GPC prepared with MK as a binder, shows more density dense concrete than that of metakaolin GGBS as a binder. The particle shape and size of ingredients of GPC have greater influence in fresh and mechanical performances enhancement of GPC. MK has high fineness resulting in enhanced workability [35]. Aggregate content in the polymer paste affects the fresh property of GPC, such as workability. When silicate reacts with free Na^+ ions in the gel, it undergoes soluble phases of NASH gel due to excess KOH cracks developed in the matrix [36]. The particle shape of the binder has a more significant impact on the structure performances of GPC. Metakaolin was observed to be irregular than spherical shape along with an edged shape leading to a lower slump [37]. Higher concentration of molarity significances that intensification in the viscosity of KOH. As the molarity of an activator is increased, the slump performances lower [38]. Higher content of SiO_2 in Metakaolin led to the rapid development of the setting timing due to the formation of the C-A-S-H structure, which tends to reduce the SV. Metakaolin indicates heterogeneous microstructure and particles from an agglomeration and makes dense with diverse particles. MK and marble are rich in SiO_2 and CaO ions with increment KS/KH molar ratio during synthesis progression. MK reacts with silica led to the formation of a novel crystalline phase [39,40]. Alkali fusion of MK, some mineral phases transformed into amorphous, and new crystalline phases formed in the GPC. Unreacted ions of Na + defined their paths in this way, either agglomerated or migrated at the boundary of remained. Metakaolin particles become less dense after the fusion process [41].

3.2. *Compression strength (CS)*

As per IS 516 code [42], the CS test was performed in a compression testing machine (CTM) with a 150 mm^3 specimen size. The CS values for different proportions of GPC tested for the 7, 14, 28, and 90 days as shown in Fig. 6a–d.

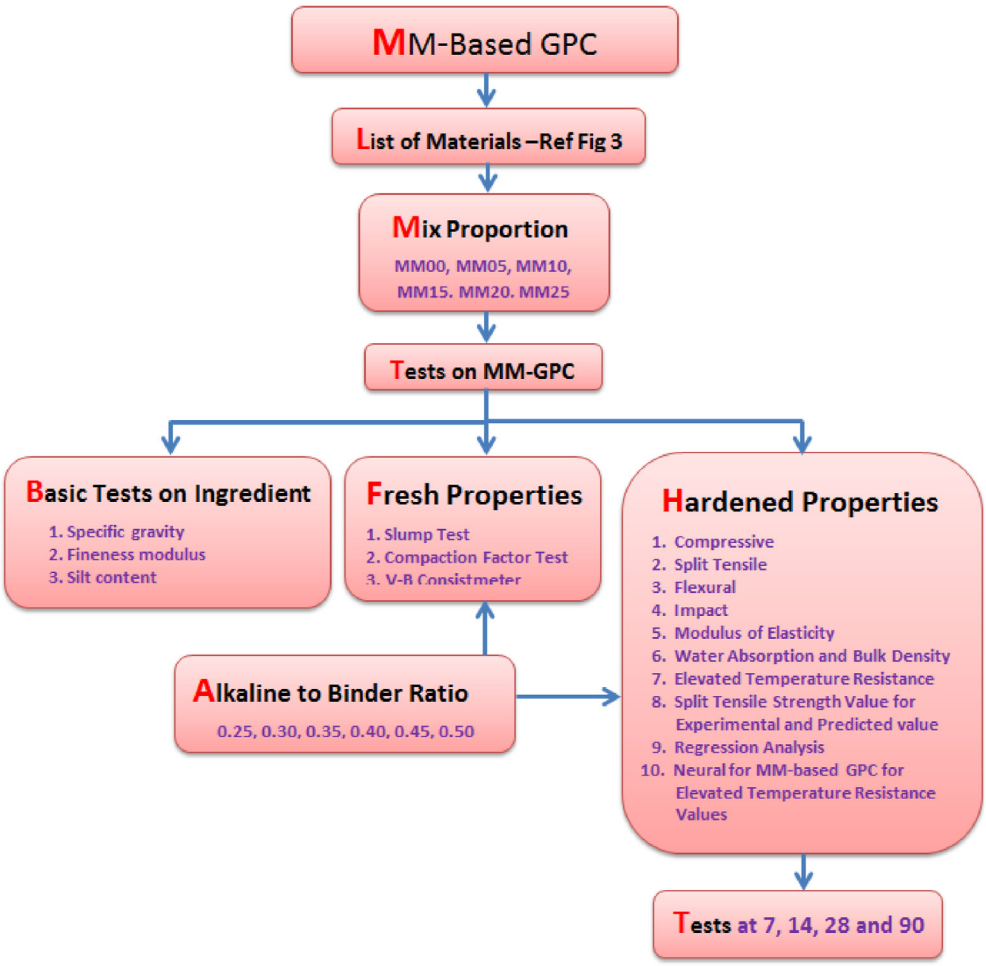

Fig. 4 – Flow chart for methodology of marble-metakaolin (MM) based GPC.

The GPC was placed in the three-layer mixture into the cubes. Each layer was compacted with a tamping rod with 35 strokes. After filling GPC into cubes, these cubes were compaction using a table vibrator before the final concrete set. CTM with a capacity of 2000 N and a 140 kg/cm^2/min loading rate was employed for crushing concrete.

To determine CS results, GPC was cast for different ratios A/B ranging from 0.25 to 0.50, with an interval of 0.05 see Fig. 6a. CS value observed after experimentation ranging from 30 (minimum) to 45 (maximum) MPa, for day 7. For an A/B ratio of 0.25, CS value was observed from 34 to 40 MPa as the minimum and maximum value. The MM00 was the mix for which maximum CS was observed as 40 MPa, and MM25 mix minimum CS was observed as 34 MPa. For an A/B ratio of 0.30, CS value was observed from 36 to 42 MPa as the minimum and maximum value. The MM00 was the mix for which maximum CS was observed as 42 MPa, and MM25 mix minimum CS was observed as 36 MPa. For an A/B ratio of 0.35, CS value was observed from 39 to 45 MPa as the minimum and maximum value. The MM00 was the mix for which maximum CS was

Table 3 – Mix proportions of GPC.

Mix ID	Binder		Fine Aggregate (kg/m^3)	Coarse Aggregate (kg/m^3)	Alkali/Binder Ratio	Alkaline Solution	
	Metakaolin (%)	Marble (%)				KOH (kg/m^3)	K_2SiO_3 (kg/m^3)
MM00	100	0	552	1290	0.25	14.66	52.4
MM05	95	05	552	1290	0.30	14.66	52.4
MM10	90	10	552	1290	0.35	14.66	52.4
MM15	85	15	552	1290	0.40	14.66	52.4
MM20	80	20	552	1290	0.45	14.66	52.4
MM25	75	25	552	1290	0.50	14.66	52.4

Table 4 – Impact energy for various mixes.

Mix ID	1st crack blows	Failure crack blows	Impact Energy- Nm
MM00	20	125	1960.17
MM05	31	135	1862.93
MM10	43	140	1747.43
MM15	36	138	1623.94
MM20	24	85	1430.45
MM25	21	60	1247.31

observed as 45 MPa, and MM25 mix minimum CS was observed as 39 MPa. For an A/B ratio of 0.40, CS value was observed from 37 to 44 MPa as the minimum and maximum value. The MM00 was the mix for which maximum CS was observed as 44 MPa, and MM25 mix minimum CS was observed as 37 MPa. For an A/B ratio of 0.45, CS value was observed from 32 to 39 MPa as the minimum and maximum value. The MM00 was the mix for which maximum CS was observed as 32 MPa, and MM25 mix minimum CS was observed as 39 MPa. For an A/B ratio of 0.50, the CS value was seen from 30 to 37 MPa as the minimum and maximum value. The MM00 was the mix for which maximum CS was observed as 37 MPa, and MM25 mix minimum CS was observed as 30 MPa.

To determine CS results, GPC was cast for different ratios A/B ranging from 0.25 to 0.50, with the interval of 0.05 shown in Fig. 6b. CS value observed after experimentation ranging from 30 (minimum) to 45 (maximum) MPa, for day 14. For an A/B ratio of 0.25, CS value was observed from 35 to 42 MPa as the minimum and maximum value. For MM00 was the mix for which maximum CS was observed as 42 MPa, and MM25 mix minimum CS was observed as 35 MPa. For an A/B ratio of 0.30, CS value was observed from 37 to 44 MPa as the minimum and maximum value. MM00 was the mix for which maximum CS was observed as 44 MPa, and MM25 mix minimum CS was observed as 37 MPa. For an A/B ratio of 0.35, CS value was observed from 44 to 50 MPa as the minimum and maximum value. For MM00 was the mix for which maximum CS was observed as 50 MPa, and MM25 mix minimum CS was observed as 44 MPa. For an A/B ratio of 0.40, CS value was observed from 42 to 49 MPa as the minimum and maximum value. MM00 was the mix for which maximum CS was observed as 49 MPa, and MM25 mix minimum CS was observed as 42 MPa. For an A/B ratio of 0.45, CS value was observed from 39 to 45 MPa as the minimum and maximum

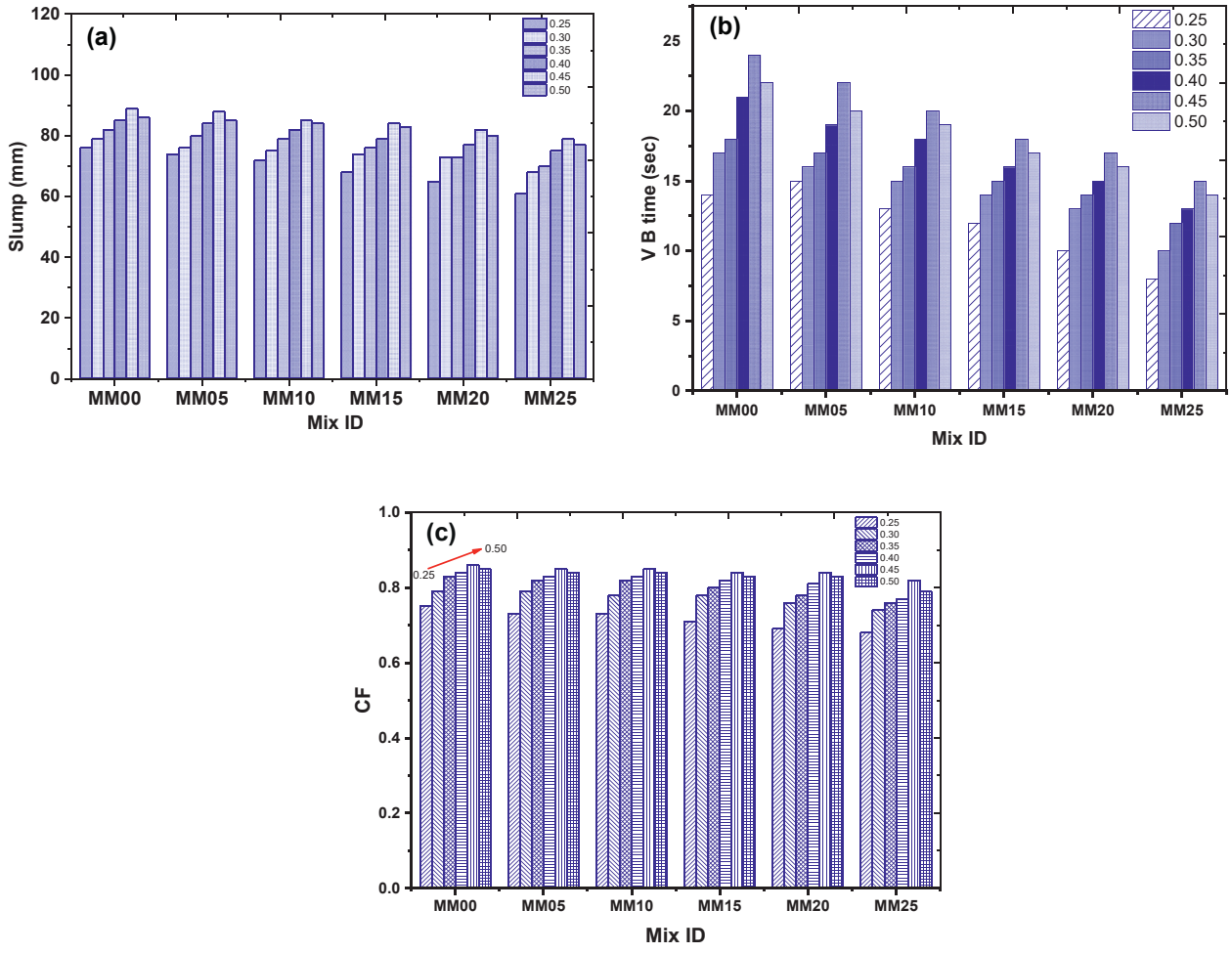

Fig. 5 – a. Slump results for different values of the A/B ratio. b. V–B consistometer results for different values of A/B ratio. c. Compaction factor results for different values of A/B ratio.

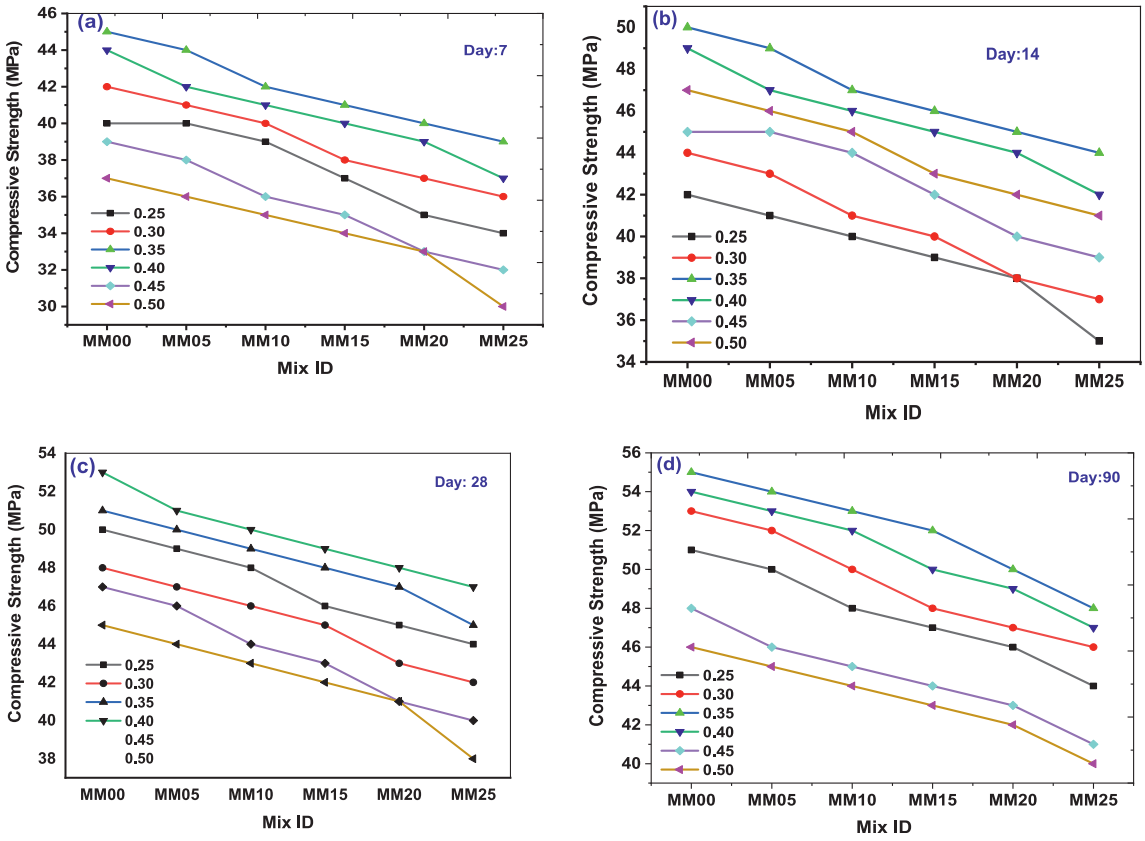

Fig. 6 – a. CS results for day 7 with various A/B ratio. b. CS results for day 14 with various A/B ratio. c. CS results for day 28 with various A/B ratio. d. CS results for day 90 with various A/B ratio.

value. MM00 was the mix for which maximum CS was observed as 45 MPa, and MM25 mix minimum CS was observed as 39 MPa. For an A/B ratio of 0.50, the CS value was obtained after experimentation, ranging from 41 to 47 MPa as the minimum and maximum values. MM00 was the mix for which maximum CS was observed as 47 MPa, and MM25 mix minimum CS was observed as 41 MPa.

Similarly, as in previous cases, determine CS results, GPC were cast for different ratios A/B ranging from 0.25 to 0.50, with the interval of 0.05 shown in Fig. 6c. CS value observed after experimentation ranging from 40 (minimum) to 53 (maximum) MPa, for day 28. For an A/B ratio of 0.25, CS value was observed from 44 to 50 MPa as the minimum and maximum value. MM00 was the mix for which maximum CS was observed as 50 MPa, and MM25 mix minimum CS was observed as 44 MPa. For an A/B ratio of 0.30, CS value was observed from 42 to 48 MPa as the minimum and maximum value. MM00 was the mix for which maximum CS was observed as 48 MPa, and MM25 mix minimum CS was observed as 42 MPa. For an A/B ratio of 0.35, CS value was observed from 45 to 51 MPa as the minimum and maximum value. MM00 was the mix for which maximum CS was observed as 51 MPa, and MM25 mix minimum CS was observed as 45 MPa. For an A/B ratio of 0.40, CS value was observed from 47 to 53 MPa as the minimum and maximum value. MM00 was the mix for which maximum CS was observed as 53 MPa, and MM25 mix minimum CS was observed as 47 MPa. For an A/B ratio of 0.45, CS value was observed from 40 to 47 MPa as the minimum and maximum value. MM00 was the mix for which maximum CS was observed as 47 MPa, and MM25 mix minimum CS was observed as 40 MPa. For an A/B ratio of 0.50, CS value was obtained after experimentation, ranging from 38 to 45 MPa as the minimum and maximum value. MM00 was the mix for which maximum CS was observed as 45 MPa, and MM25 mix minimum CS was observed as 38 MPa.

Following the CS results, GPC was cast for different ratios A/B ranging from 0.25 to 0.50, with the interval of 0.05 shown in Fig. 6d. CS value observed after experimentation ranging from 40 (minimum) to 55 (maximum) MPa, for day 90. For an A/B ratio of 0.25, CS value was observed from 44 to 51 MPa as the minimum and maximum value. MM00 was the mix for which maximum CS was observed as 51 MPa, and MM25 mix minimum CS was observed as 44 MPa. For an A/B ratio of 0.30, CS value was observed from 46 to 53 MPa as the minimum and maximum value. MM00 was the mix for which maximum CS was observed as 53 MPa, and MM25 mix minimum CS was observed as 46 MPa. For an A/B ratio of 0.35, CS value was observed from 48 to 55 MPa as the minimum and maximum value. MM00 was the mix for which maximum CS was observed as 55 MPa, and MM25 mix minimum CS was observed as 48 MPa. For an A/B ratio of 0.40, CS value was observed from 47 to 54 MPa as the minimum and maximum value. MM00 was the mix for which maximum CS was

observed as 54 MPa, and MM25 mix minimum CS was observed as 47 MPa. For an A/B ratio of 0.45, CS value was observed from 41 to 48 MPa as the minimum and maximum value. MM00 was the mix for which maximum CS was observed as 48 MPa, and MM25 mix minimum CS was observed as 41 MPa. For an A/B ratio of 0.50, CS value was obtained after experimentation, ranging from 40 to 46 MPa as the minimum and maximum value. MM00 was the mix for which maximum CS was observed as 46 MPa, and MM25 mix minimum CS was observed as 40 MPa.

A total of six samples were taken and analyzed over 7, 14, 28, and 90 days to determine CS. The average of the tested specimen findings was recorded, and they are all represented in Fig. 6a–d. According to a previous study, the reaction rate of GPC is much faster than the hydration rates of traditional concrete because of the tetrahedral structure. With MM100%, the mixture maximum CS was 51 MPa. The A/B ratio was increased, which boosted this number. The maximum CS strength was achieved with MM100% binder concentration.

3.2.1. *Effect of the activator and A/B on CS*

The CS and A/B ratio have a unique relationship. Initially, the A/B ratio increased to a specific range of CS increases beyond the limit. Because the KOH and KSi_2O_3 are acts as an alkaline agent, it produces more SiO_2 gel from MK, and GGBS stimulates the formation of denser Si–O–Si linkages during polymerization. The Si–O–Si connection, on the other hand, is much stronger than the Si–O–Al and Al–O–Al bonds. As a result, CS is enhanced. The NaOH solution detaches the SiO_2 and Al_2O_3 in the matrix, leading to the monomer to polymer bond formation [10,14,43]. The influence of the A/B ratio on CS is shown in Fig. 6. The CS of a combination containing a marble powder MM100% -based GPC increases when the A/B ratio increases from 0.25 to 0.35, then decreases (in A/B ratio 0.50). The best A/B ratio was different to produce maximum CS for each combination type [44]. As a result, it was discovered that the A/B ratio had a strong association with binder chemical composition since binder were rich in SiO_2 and Al_2O_3 content, which led to strength development, causing acceleration of the rate of geopolymerization. The strength of compression the CS of marble-Metakaolin based GPC develop with a parameter such as A/B ratio to a particular value reflecting the optimum-active ratio of A/B and then drops more or less than this value [45].

Under extremely hot conditions, a comparison of FA based GPC with NaOH and KOH activators was investigated. According to the findings, KOH based activators agent led to produce GPC with higher CS than NaOH. The KOH is appropriate for structural uses. This is due to the better binding properties of KOH with GPC than NaOH activators [46]. Compared to Na activators, KOH offers greater strength and durability with little quantity to accelerate the geopolymerization reaction. Additionally, $KSiO_2$ has less viscosity than Na_2SiO_3 [47]. Potassium alkali agent decreased viscosity results in greater strength and durability with less shrinkage and porosity [50,51]. When compared the curing condition of GPC with ambient and oven-cured conditions, it was concluded that the oven curing condition shows a higher CS value than the ambient condition [48]. When the A/B ratio surpasses the active-optimum value, the activator agent skips over the demands of the Geopolymerization process, resulting in decreased CS [49–51]. For mixes (MM00, MM05, MM10, MM15, MM20, and MM25), the optimum A/B ratio that provided the maximum CS was (0.35, 0.30, 0.25, 0.40, and 0.50).

3.3. *Spit tensile strength (STS)*

As per IS 5816 code [52], the STS test was carried out in a CTM with a 150 × 300 mm cylinder specimen. GPC testing for STS was carried out for 7, 14, 28, and 90 days are shown in Fig. 7a–d (results summarized in Table 5). IS 5816 was validated by a split tensile test. The cylinder measures 150 (Dia.) x 300 (Ht.) mm in dimension. The cylinder was tested using a CTM with a 1.2–2.4 N/(mm/min) load rate. Eq (1) is a formula for the computation of STS.

$$Fc = \frac{2P}{\pi LD} \tag{1}$$

where, $\pi = 3.142$, Fc-measured STS -maximum Load (N), L-length of the specimen, D-cross-sectional diameter of the specimen.

STS value observed after experimentation ranging from 3.05 (minimum) to 4.35 (maximum) MPa, for day 7, refer Fig. 7a for A/B ratios ranging from 0.25 to 0.50. For the A/B ratio of 0.25, the STS value was observed from 3.25 to 4.15 MPa as the minimum and maximum value.

Fig. 7a indicates STS results of GPC for day 7, for various values of A/B ratios of 0.25–0.50. The STS value reduced as the A/B ratios increased from 0.25 to 0.50. For the A/B ratio of 0.35, a maximum STS value was observed. From the binder point of view, the marble content increases, the STS value reduces. MM00 has 0% marble; maximum STS was observed for an A/B ratio of 0.35. For an A/B ratio of 0.50, CS value was observed from 3.05 to 3.85 MPa as the minimum and maximum value. MM00 was the mix for which maximum STS was observed as 3.85 MPa, and MM25 mix minimum STS was observed as 3.05 MPa when tested for day 7. STS value observed for MM00 mix is 12%,10.1% 12.98% 10.95%, 8% and 9.2% higher than MM25 mix for A/B ratio ranging from 0.25 to 0.50 respectively. MM00 for A/B ratio of 0.35 has a 12.98% higher STS value than MM25.

STS value observed after experimentation ranging from 3.08 (minimum) to 4.48 (maximum) MPa, for day 14, refer to Fig. 7b. For the A/B ratio of 0.25, the STS value was observed from 3.28 to 4.08 MPa as the minimum and maximum value. Fig. 7b indicates STS results of GPC for day 14, for various values of A/B ratios of 0.25–0.50. The STS value reduced as the A/B ratios increased from 0.25 to 0.50. For the A/B ratio of 0.35, a maximum STS value was observed. From the binder point of view, the marble content increases, the STS value reduces. MM00 has 0% marble; maximum STS was observed for an A/B ratio of 0.35. MM00 was the mix for which maximum STS was observed as 4.38 MPa, and MM25 mix minimum STS was observed as 3.58 MPa.For the A/B ratio of 0.50, the STS value was observed from 3.08 to 3.78 MPa as the minimum and maximum value. MM00 was the mix for which maximum STS was seen as 3.78 MPa, and MM25 mix minimum STS was observed as 2.08 MPa. STS value was seen for MM00 mix value is 7.3%, 5.1%, 7.9%, 8.15%, 8.3%, and 6% higher than MM25 mix

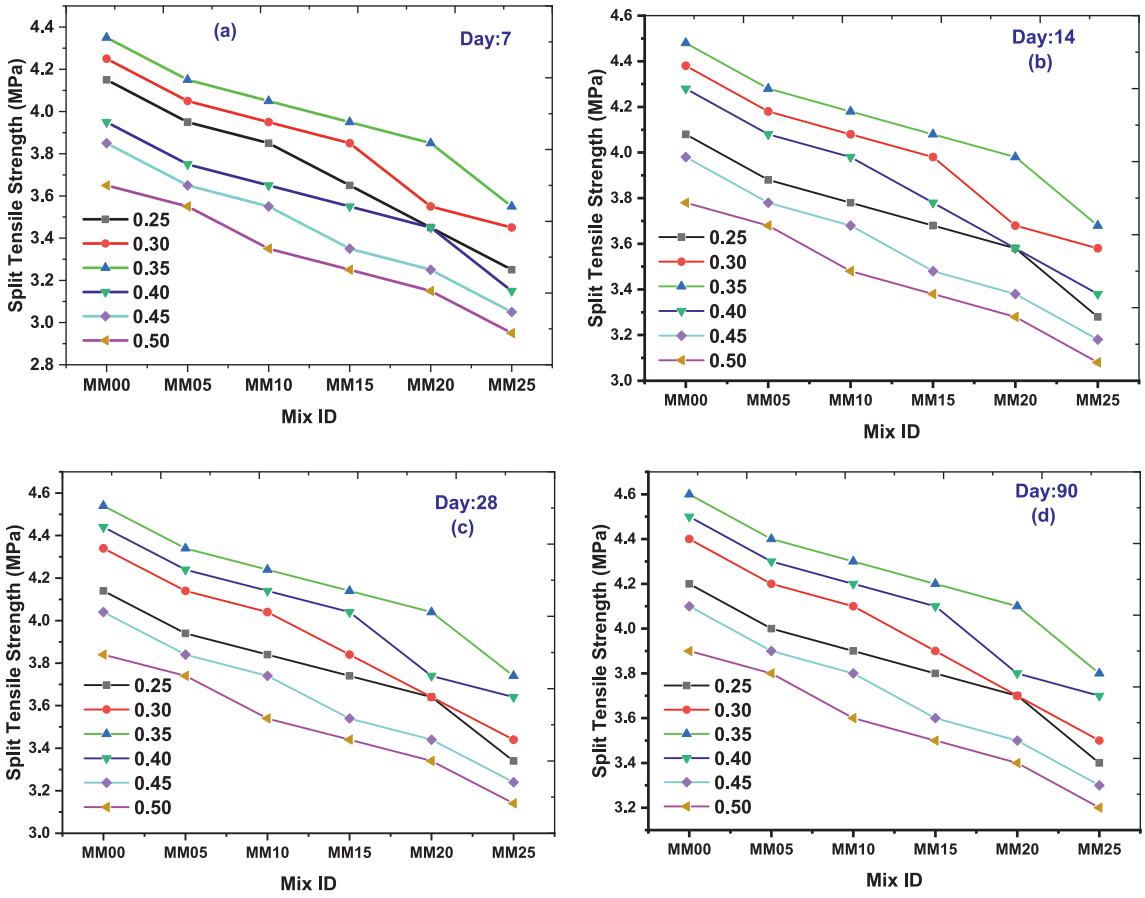

Fig. 7 – a. Variation of STS data for day 7, with various A/B ratios. b. Variation of STS data for day 14, with various A/B ratios. c. Variation of STS data for day 28, with various A/B ratios. d. Variation of STS data for day 90, with various A/B ratios.

for A/B ratio ranging from 0.25 to 0.50 respectively. MM00 for A/B ratio of 0.35 has a 7.9% higher STS value than MM25.

STS value observed after experimentation ranging from 3.14 (minimum) to 4.54 (maximum) MPa, for day 28, refer Fig. 7c for A/B ratios ranging from 0.25 to 0.50. Fig. 7c indicates STS results of GPC for day 28, for various values of A/B ratios of 0.25–0.50. The STS value reduced as the A/B ratios increased from 0.25 to 0.50. For the A/B ratio of 0.35, a maximum STS value was seen. From the binder point of view, the marble content increases, the STS value reduces. MM00 has 0% marble; maximum STS was seen for an A/B ratio of 0.35. For an A/B ratio of 0.25, the STS value was seen from 3.34 to 4.14 MPa as the minimum and maximum value. For MM00 was the mix for which maximum STS was seen as 4.14 MPa, and MM25 mix minimum STS was seen as 3.34 MPa. For the A/B ratio of 0.50, the STS value was seen from 3.14 to 3.84 MPa as the minimum and maximum value. MM00 was the mix for which maximum STS was seen as 3.84 MPa, and MM25 mix minimum STS was seen as 3.14 MPa.STS value was seen for MM00 mix value is 7%, 5% 7.8%, 8%, 8.2%, and 5.9% higher than MM25 mix for A/B ratio ranging from 0.25 to 0.50 respectively. MM00 for A/B ratio of 0.35 has a 7.8% higher STS value than MM25.

STS value observed after experimentation ranging from 3.2 (minimum) to 4.56 (maximum) MPa, for day 90, refer Fig. 7d for A/B ratios ranging from 0.25 to 0.50. Fig. 7b indicates STS results of GPC for day 90, for various values of A/B ratios of 0.25–0.50. The STS value reduced as the A/B ratios increased from 0.25 to 0.50. For the A/B ratio of 0.35, a maximum STS value was observed. From the binder point of view, the marble content increases, the STS value reduces. MM00 has 0% marble. MM00 was the mix for which maximum STS was observed as 4.4 MPa, and MM25 mix minimum STS was observed as 3.5 MPa For the A/B ratio of 0.50, the STS value was seen from 3.2 to 3.9 MPa as the minimum and maximum value. For MM00 was the mix for which maximum STS was observed as 3.9 MPa, and MM25 mix minimum STS was observed as 3.2 MPa. STS value was observed for MM00 mix value is 7.1%, 5%,7.6%, 7.8%,8.1%, and 5.8% higher than MM25 mix for A/B ratio ranging from 0.25 to 0.50 respectively. MM00 for A/B ratio of 0.35 has a 7.6% higher STS value than MM25.

3.3.1. *Effect of activators on STS*

As the ratio of (KS/KH) was increased from 0.25 to 0.50, the STS value decreased (more details see Table 5). For KS/KH ratio of 0.35, maximum STS value was observed for 7,14,28 and 90 days of testing. It was also observed that percentage increment of STS value from 90 days of testing to 7 days were in the range from 0.60 to 1.0 MPa MM00 i. e, MK as binder with 100%, shows maximum STS, but as the percentage of marble powder was increased the STS value will deline. The curing condition and the K_2SiO_3 and KOH (KS/KH) ratio influence the STS of the GPC. The maximum STS for varied KS/KH ratios ranging from

Table 5 – Comparison of STS results values for various codes and proposed empirical formula.

Study	Expt.CS	Expt.STS	IS-code	AS3600	CEB-FIP	ACI 363	Verma and Dev	Proposed	Ref.
Current Study	55.0	4.60	5.19	2.97	4.22	4.38	7.54	4.62	
	54.0	4.40	5.14	2.94	4.17	4.34	7.43	4.58	
	53.0	4.30	5.10	2.91	4.12	4.30	7.32	4.53	
	52.0	4.20	5.05	2.88	4.07	4.25	7.21	4.48	
	50.0	4.10	4.95	2.83	3.97	4.17	6.98	4.38	
	48.0	3.80	4.85	2.77	3.86	4.09	6.76	4.28	
0.00	58.2	5.54	5.34	3.05	4.51	2.14	7.88	4.77	[92]
	49.5	4.82	4.92	2.82	4.05	1.97	6.93	4.36	
	35.4	2.79	4.16	2.38	3.23	1.67	5.30	3.60	
	28.9	2.66	3.76	2.15	2.38	1.51	4.51	3.21	
	46.1	4.00	4.75	2.72	3.86	1.90	6.54	4.18	
	36.1	3.81	4.21	2.40	3.28	1.68	5.38	3.64	
	40.4	4.14	4.45	2.54	3.54	1.78	5.89	3.88	
	41.3	4.19	4.50	2.57	3.59	1.80	5.99	3.93	
	33.5	3.37	4.05	2.32	3.12	1.62	5.07	3.49	
	30.5	3.57	3.87	2.21	2.93	1.55	4.70	3.31	
	35.1	3.28	4.15	2.37	3.21	1.66	5.26	3.59	
	37.1	3.26	4.26	2.44	3.34	1.71	5.50	3.70	
	37.6	3.60	4.29	2.46	3.37	1.72	5.56	3.73	
	35.2	3.20	4.15	2.37	3.22	1.66	5.28	3.59	
1.00	28.5	2.10	3.74	2.34	3.16	1.64	4.46	3.19	[20]
	36.6	3.20	4.23	2.33	3.13	1.63	5.44	3.67	
	47.9	4.10	4.84	2.32	3.10	1.62	6.75	4.28	
	33.1	2.60	4.03	2.30	3.08	1.61	5.02	3.47	
	45.3	2.20	4.71	2.29	3.05	1.60	6.45	4.14	
	43.8	2.50	4.63	2.27	3.02	1.59	6.28	4.07	
2.00	44.0	3.60	4.64	2.26	2.99	1.58	6.31	4.08	[87]
	46.0	3.90	4.75	2.24	2.96	1.57	6.53	4.18	
	47.0	4.00	4.80	2.23	2.93	1.56	6.65	4.23	
	54.0	4.10	5.14	2.21	2.90	1.55	7.43	4.58	
	46.0	3.00	4.75	2.20	2.88	1.54	6.53	4.18	
	44.0	3.60	4.64	2.18	2.85	1.53	6.31	4.08	
	42.0	3.50	4.54	2.17	2.82	1.52	6.08	3.97	
3.00	20.3	2.70	3.15	2.16	2.79	1.51	3.40	2.63	[92]
	24.0	3.50	3.43	2.14	2.76	1.50	3.88	2.89	
	25.0	3.60	3.50	2.13	2.73	1.49	4.01	2.96	
	25.4	3.80	3.53	2.11	2.70	1.48	4.06	2.99	
	25.8	4.00	3.56	2.10	2.68	1.47	4.12	3.01	
4.00	21.2	2.92	3.22	2.08	2.65	1.46	3.52	2.70	[93]
	25.3	3.14	3.52	2.07	2.62	1.45	4.05	2.98	
	33.3	3.34	4.04	2.05	2.59	1.44	5.04	3.48	
	44.3	4.41	4.66	2.04	2.56	1.43	6.34	4.09	
	25.3	3.18	3.52	2.03	2.53	1.42	4.05	2.98	
	30.2	3.95	3.84	2.01	2.50	1.41	4.66	3.29	
	46.3	4.21	4.76	2.00	2.48	1.40	6.56	4.19	
	48.3	4.75	4.86	1.98	2.45	1.39	6.79	4.29	
5.00	65.0	2.30	5.64	1.97	2.42	1.38	8.61	5.08	[46]
	72.0	3.50	5.94	1.95	2.39	1.37	9.35	5.38	
	74.0	3.67	6.02	1.94	2.36	1.35	9.55	5.47	
	60.0	2.08	5.42	1.92	2.33	1.34	8.08	4.86	
	66.0	3.32	5.69	1.91	2.30	1.33	8.72	5.13	
	65.0	3.47	5.64	1.89	2.28	1.32	8.61	5.08	
	53.0	4.00	5.10	1.88	2.25	1.31	7.32	4.53	
	57.0	4.32	5.28	1.87	2.22	1.30	7.75	4.72	
	59.0	4.58	5.38	1.85	2.19	1.29	7.97	4.81	

0.5 to 3.0 with intervals of 0.5 at 90 days for ambient-curing is in the range of 2.7–3.6 MPa. At 90 days of ambient curing, the maximum STS for varied KS/KH ratios ranging from 0.5 to 3.0 with intervals of 0.5 is in the range of 3.5–5.0 MPa. Compared to lower molarity, GPC performance for STS improves with increasing molarity. In comparison to standard concrete specimens, the potassium activator-based GPC exhibits significant strength qualities. This is because the reaction between aluminium silicate components and an alkaline solution gives GPC an excellent binding property and boosts its STS [50,53]. The activator requires an alkaline compound in an aqueous form. The mixture of silicates and hydroxides is

often employed. The resulting solution's silicate serves as an additional source of SiO_2, while the hydroxide ensures the solution's high alkalinity. The alkaline solution is vital during geopolymerization and influences STS growth. The SiO_2/Al_2O_3 ratio, the efficacy of the geopolymerization reaction, kind of cation utilized, molar concentration, and curing conditions all significantly impact the STS of geopolymers [54–56].

On the other hand, SiO_2/Al_2O_3 were engaged in the formation of CSH and CASH gel, improving mechanical strength. The STS of samples activated with 12 M NaOH solution was 5.12 MPa, which was greater than the STS of samples activated with higher or lower molarity solutions, which were 4.43 and 5.08 MPa, respectively, for 10 M and 14 M. The most essential are reactive silica content and particle size (Ganachari, 2019). Changes in the quantity of SiO_2 and Al_2O_3, according to specific research, have a considerable effect on the characteristics of the geopolymers. Reactivity of the binder and the chemical composition of the activator is required for the speedy acceleration of the geopolymerization process [57].

3.4. *Flexural strength*

Flexural strength (FS) test was conducted as per IS 516 code [42], in UTM. The FS test was performed following IS 516 specifications. 100 × 100 × 500 mm was taken as the specimen size. Load of 180 kg/cm^2/min was applied to the specimen up to it failed.

$$FS = \frac{PL}{(B\,D\,\hat{}\,2)} \quad (2)$$

P-Failure load of the specimen, L-Length of the specimen-Width of the specimen.

D-Depth of the specimen.

After subjecting the beam under UTM, failure crack is observed in beam specimen refer to Fig. 8a–d. After viewing Fig. 8c, it is clear that maximum impact was observed at the central portion of the beam. Failure of the beam has taken place at the mid-span of the beam. Fig. 9 shows the cross-section of the beam. Fig. 9b closed-loop observed are aggregate and surrounded by GPC matrix.

Beams were cast to calculate FS for A/B ratios ranging from 0.25 to 0.50, with a 0.05 interval. Fig. 10a shows the FS value following testing, ranging from 3.05 (minimum) to 4.35 (highest) MPa on day 7. Fig. 10a shows GPC FS findings on day 7 for different A/B ratios ranging from 0.25 to 0.50. The STS value decreased as the A/B ratios increased from 0.25 to 0.50. A maximum FS value was obtained for the A/B ratio of 0.35. The marble content increases as the FS value decreases from the binder's perspective. The maximum STS was found with an A/B ratio of 0.35 in MM00, with 0% marble. The minimum and highest FS values were recorded for an A/B ratio of 0.50, ranging from 3.38 to 4.08 MPa.

The highest FS for MM00 was found to be 4.08 MPa, and the minimum FS for MM25 was found to be 3.38 MPa. For A/B ratios ranging from 0.25 to 0.50, the FS value observed for MM00 mix is 9.3%, 5%, 7.6%, 7.8%, 8.1%, and 5.8% greater than MM25 mix. MM00 has a 7.6% higher FS value than MM25 for an A/B ratio of 0.35.

FS for A/B ratios ranging from 0.25 to 0.50, with a 0.05 interval. Fig. 10b shows that the FS value measured following experiments varied from 3.68 (minimum) to 4.91 (highest) MPa on day 14. Fig. 10b shows GPC FS findings for

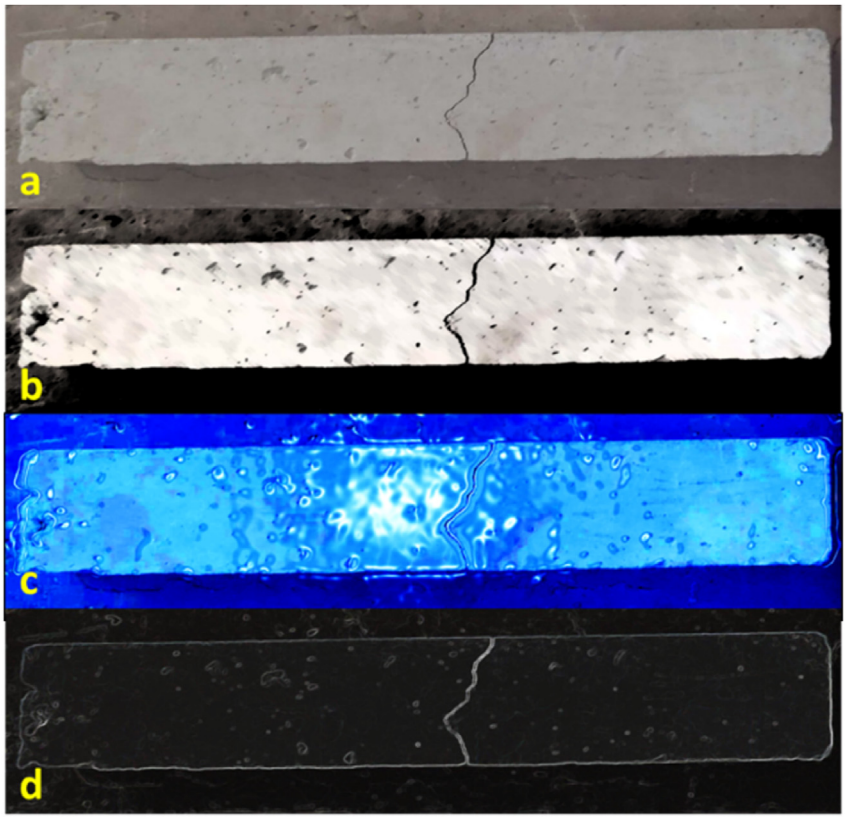

Fig. 8 – a to d. Beam cast for FS tests.

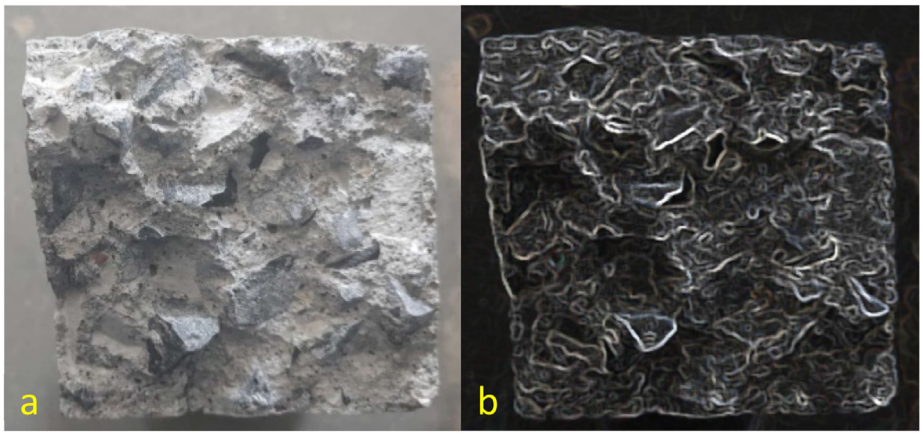

Fig. 9 – a and b. Cross-section view of the beam.

day 14 for different A/B ratios ranging from 0.25 to 0.50. The STS value decreased as the A/B ratios increased from 0.25 to 0.50. The lowest and highest FS values for the A/B ratio of 0.35 were 4.18 and 4.91 MPa, respectively. The highest FS for MM00 was found to be 4.91 MPa, and the minimum FS for MM25 was found to be 4.18 MPa. The lowest and highest FS values for an A/B ratio of 0.50 were 3.48 and 4.18 MPa, respectively. The highest FS for MM00 was found to be 4.18 MPa, and the minimum FS for MM25 was found to be 3.48 MPa. For A/B ratios ranging from 0.25 to 0.50, the FS value observed for MM00 mix is 6.6%, 4.6%, 7.1%, 7.3%, 7.5%, and 5.4%, respectively, greater than MM25

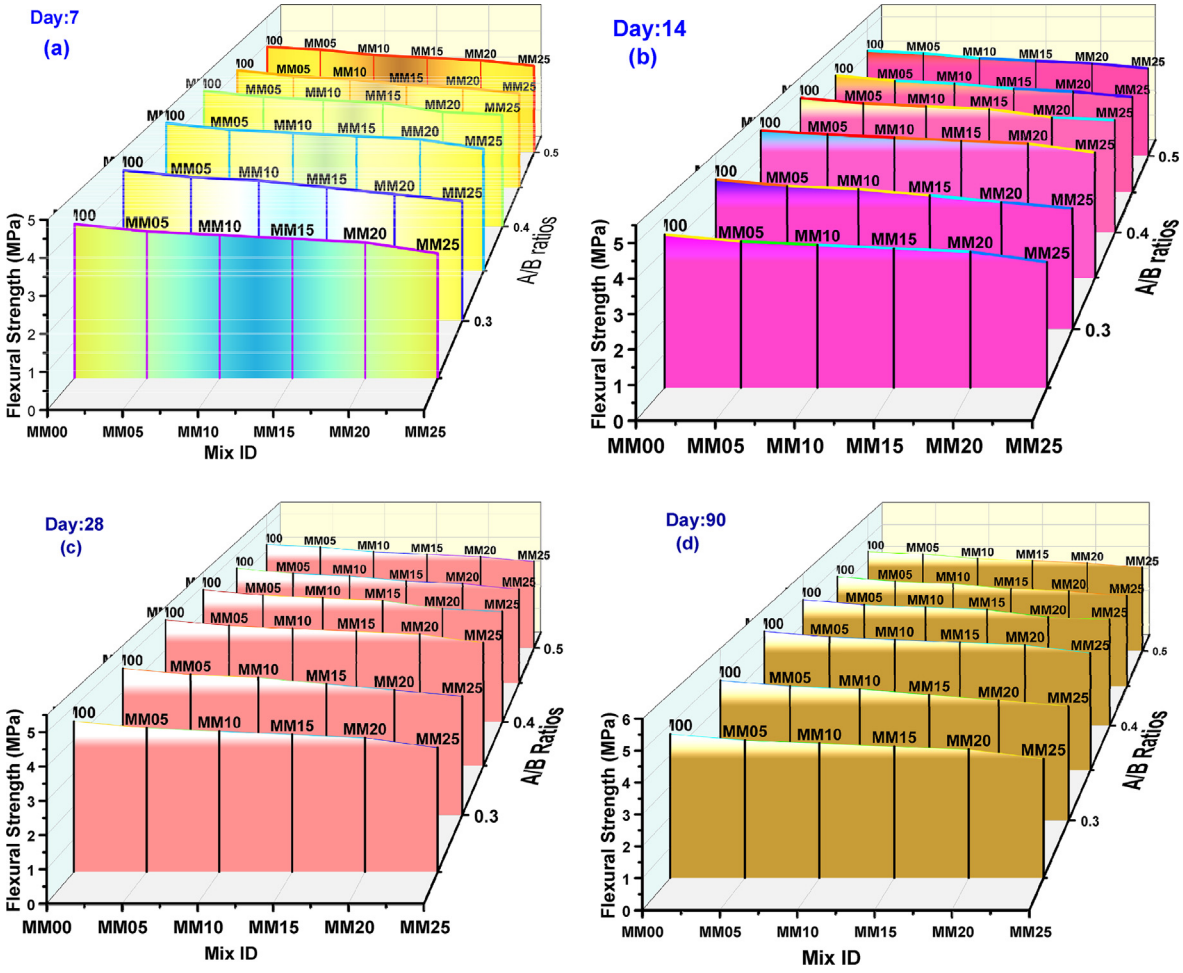

Fig. 10 – a. FS results for different values of A/B ratios. b. FS results for different values of A/B ratio day 14. c. FS results for different values of A/B ratios day 28. d. FS results for different values of A/B ratios day 90.

mix. MM00 has a 12.98% higher FS value than MM25 for an A/B ratio of 0.35.

FS for A/B ratios ranging from 0.25 to 0.50, with a 0.05 interval. Fig. 10c shows the FS value following testing, ranging from 3.68 (minimum) to 4.91 (maximum) MPa on day 28. Fig. 10c shows GPC FS findings for day 28 for different A/B ratios ranging from 0.25 to 0.50. As the A/B ratios grew from 0.25 to 0.50, the STS value decreased. The lowest and highest FS values for the A/B ratio of 0.35 were 4.24 and 5.04 MPa, respectively. The highest FS for MM00 was found to be 5.04 MPa, and the minimum FS for MM25 was found to be 4.24 MPa. The lowest and highest FS values for an A/B ratio of 0.50 were 3.56 and 4.26 MPa, respectively. The highest FS for MM00 was found to be 4.26 MPa, and the minimum FS for MM25 was found to be 3.56 MPa. For A/B ratios ranging from 0.25 to 0.50, the FS value observed for MM00 mix is 6.5%, 4.5%, 7%, 7.2%, 7.3%, and 5.3%, respectively, higher than MM25 mix. The FS value of MM00 with an A/B ratio of 0.35 is 7% higher than that of MM25.

FS for A/B ratios ranging from 0.25 to 0.50, with a 0.05 interval. Fig. 10d shows the FS value following testing, ranging from 3.68 (minimum) to 5.15 (highest) MPa on day 90. Fig. 10d shows GPC FS findings for day 28 for different A/B ratios ranging from 0.25 to 0.50. As the A/B ratios grew from 0.25 to 0.50, the STS value decreased. The FS value for the A/B ratio of 0.35 ranged from 4.35 to 5.15 MPa as the minimum and highest values. The highest FS for MM00 was found to be 5.15 MPa, and the minimum FS for MM25 was found to be 4.35 MPa. The lowest and highest FS values for an A/B ratio of 0.50 were 3.68 and 4.38 MPa, respectively. The highest FS for MM00 was found to be 4.38 MPa, and the minimum FS for MM25 was found to be 3.68 MPa. For A/B ratios ranging from 0.25 to 0.50, the FS value observed for MM00 mix is 6.4%, 4.4%, 6.8%, 7%, 7.1%, and 5.1%, respectively, greater than MM25 mix. The FS value of MM00 with an A/B ratio of 0.35 is 7% higher than that of MM25.

3.4.1. *Effect of activators on FS*

Quicker dissolution of alumina and silica from the binder into the solution, allowing for the creation of higher volumes of alumino-silicate polymeric gel and hence increased mechanical strength [58]. It's also clear from the data that with the increase of A/B ratio, FS increase up to specific values, later declining. Incremental in strength development of GPC with curing age which they ascribed to the dissolution of non-complexed species such Potassium ions, which led to framework instability in the aqueous environment [59]. Due to the high shrinkage in the matrix, this matrix includes a higher quantity of unreacted MK particles. Lower water requirement and the gel environment of the binder, a better quality of GPC than conventional concrete. GPC has a lower rate of hydration while setting [60–62]. Another significant factor is the development of micro-cracks in ITZ. These micro-cracks influence FS as associated with CS, decreasing the FS with age. FS specimens were cured at ambient temperature does not withstand their weight after demoulding. Failure of beam specimens was found to be the brittle mode [63]. The presence of a more viscous activator agent reduces the amount of unreacted MK in the matrix, resulting in the formation of strong bonds between silica and alumina ions. The K_2SiO_3/KOH ratio is reduced, which causes potassium silicate to be less viscous than potassium hydroxide, resulting in a decrease in FS [36,64].

3.5. *Impact tests*

The impact resistance of cylindrical specimens was explored with a 150 × 50 mm, i.e., dia x ht. A steel ball weighing 3 kg was dropped freely from a height of 457 mm to evaluate impact resistance. Initial crack blows are the number of blows that generate a visible first crack, while failure blows are the number of blows that induce total crack propagation was noted [65,66].

Equation E = Nmgh was used to compute impact energy (Nm).

Whereas N: number of strikes that cause the specimen to fail,

m: weight of the steel ball,
h: freely falling height of the ball, and
g: acceleration due to gravity.

Fig. 11 shows the impact test results for the A/B ratio of 0.35. The impact test is performed using an A/B ratio of 0.35. since it has been experimental that this ratio shows better mechanical performances than other ratios. The impact test is the measure of impact energy that GPC resists. The MM00 mix ID shows maximum impact energy and MM25 as minimum impact energy with 1960.17 Nm and 1247.31Nm, respectively. From Fig. 11, it can be clearly seen that as marble content increases, the impact energy decrease.

3.6. *Modulus of elasticity (MoE)*

MoE was carried out as per IS 516 [42]. Concrete cylinders with a diameter of 150 cm and a length of 300 cm will be used as test specimens. Other sizes of cylinders or square prisms may also be utilised, as long as the height/diameter or height/width ratio is at least two. BEESWARM graph is plotted for representation of MoE data. For 7, 14, 28, and 90 days strength of MoE, MM00 mix shows maximum, with CS of 30–40 MPa for 90 days, MoE among all the mixes as shown in Fig. 12. As the

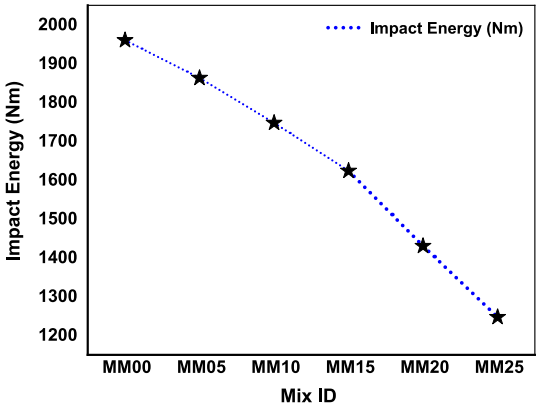

Fig. 11 – Impact tests result for different mix ID for GPC for A/B ratio of 0.35.

marble content increases in the mix, the MoE decline. As the curing day increases, the MoE also increases. From experimentation observation, MoE results for 90 days strength were marginal increases compared with 7, 14, and 28 days. A/B ratio of 0.25 shows maximum MoE among all curing days.

Several variables influence the MoE of GPC, including the kind of alkali utilized, K^+ or Na^+, chemical composition, SiO_2/Al_2O_3 ratio, curing time, and temperature [67]. An increase in MoE is due mainly to good uniformity. Furthermore, differing viscosities and alkaline silicates of different cations might affect the processes throughout the geopolymerization process, resulting in variable microstructures and mechanical characteristics [68]. The microstructure of the GPC materials produced with potassium silicate was considerably denser (less porous) than that of the sodium silicate mortars. This, in turn, impacted the longitudinal MoE. Mixed mortars made from different elemental silicates and hydroxides exhibited intermediary [69].

3.7. *Water absorption and bulk density*

Water absorption (WA) test for GPC was carried out as per ASTM c1585 [70] code. The ASTM C1585-20 standard was used to conduct the water absorption test. At room temperature, the dry weight of the GPC cubes was noted, say (A). At room temperature, cubes were soaked in clean water for 24 h. Remove the specimen and use a moist towel to wipe away any traces of water on the GPC surface. The specimen weight was recorded (B).

Eq'n 3 was used to compute the % of water absorption.

$$Water\ Absorption = (B - A)/A \times 100 \quad (3)$$

WA value observed after experimentation ranging from 8 (minimum) to 19 (maximum) %, for day 90 as shown in Fig. 13a for A/B of 0.25–0.50. The WA value ranged from 8 to 13 percent as a minimum and maximum for an A/B ratio of 0.25. The highest WA for MM25 was observed to be 13%, whereas the minimum WA for MM00 was 8%. For an A/B ratio of 0.50, the WA value ranged from 12 to 19 percent as a minimum and maximum. The highest WA for MM25 was observed to be 19%, while the minimum WA for MM00 was observed to be 12%. The WA value observed for MM25 mix is 3.33%, 3.03%, 2.8%, 2.66%, 2.9%, and 3.15% respectively, greater than MM00 mix. The WA value of MM25 with an A/B ratio of 0.50 is 3.15% higher than that of MM00.

WA value observed after experimentation ranging from 2212 (minimum) to 2316 (maximum) kg/m3 for day 90, as shown in Fig. 13b for A/B of 0.25–0.50. For an A/B ratio of 0.25, BD value was observed from 2212 to 2278 kg/m^3 as the minimum and maximum value. The maximum BD was 2278 kg/m3 for the MM25 mix, while the minimum BD was 2212 kg/m3 for the MM00 mix. With an A/B ratio of 0.50, the BD value ranged from 2250 to 2316 kg/m3 as the minimum and maximum value. Maximum BD was observed for MM25 at 2316 kg/m3,

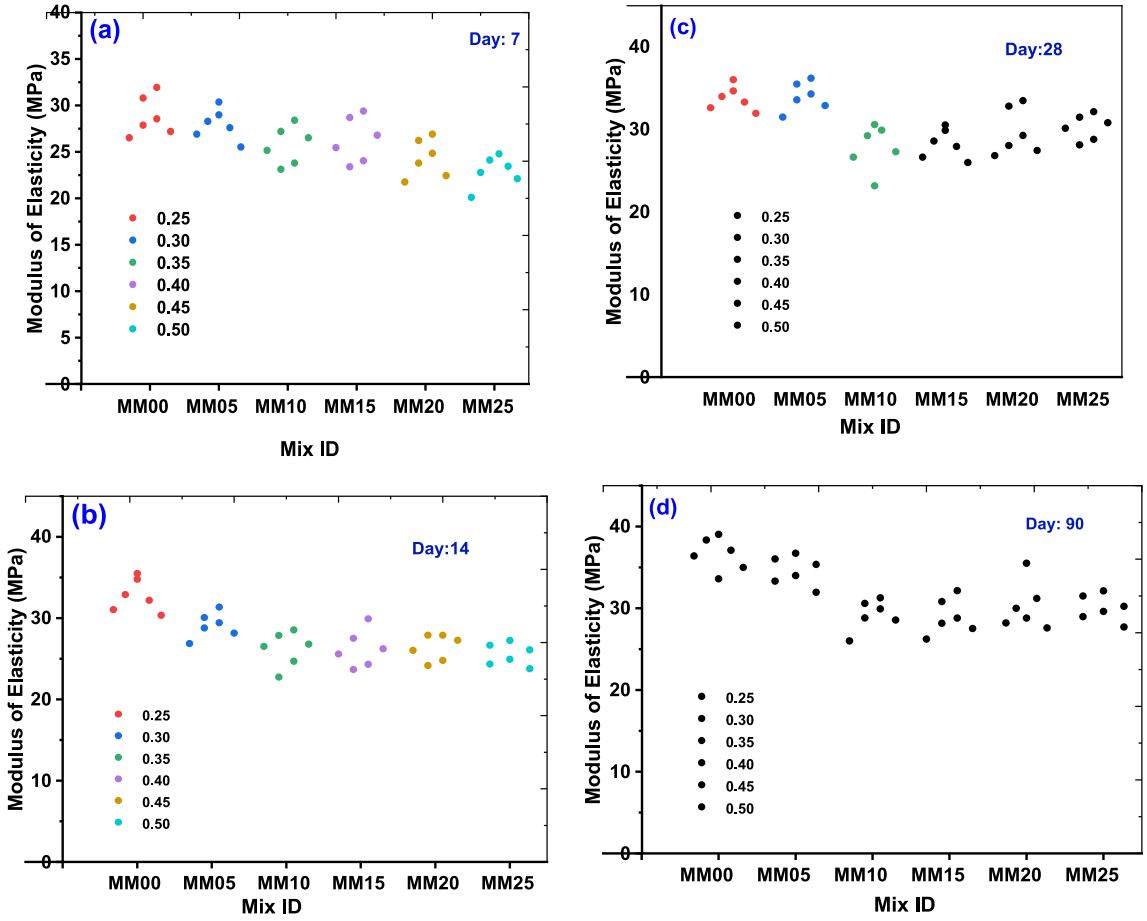

Fig. 12 – BEESWARM plots represent MoE for MK-based GPC for (a)7, (b)14, (c)28, and (d)90 days, respectively.

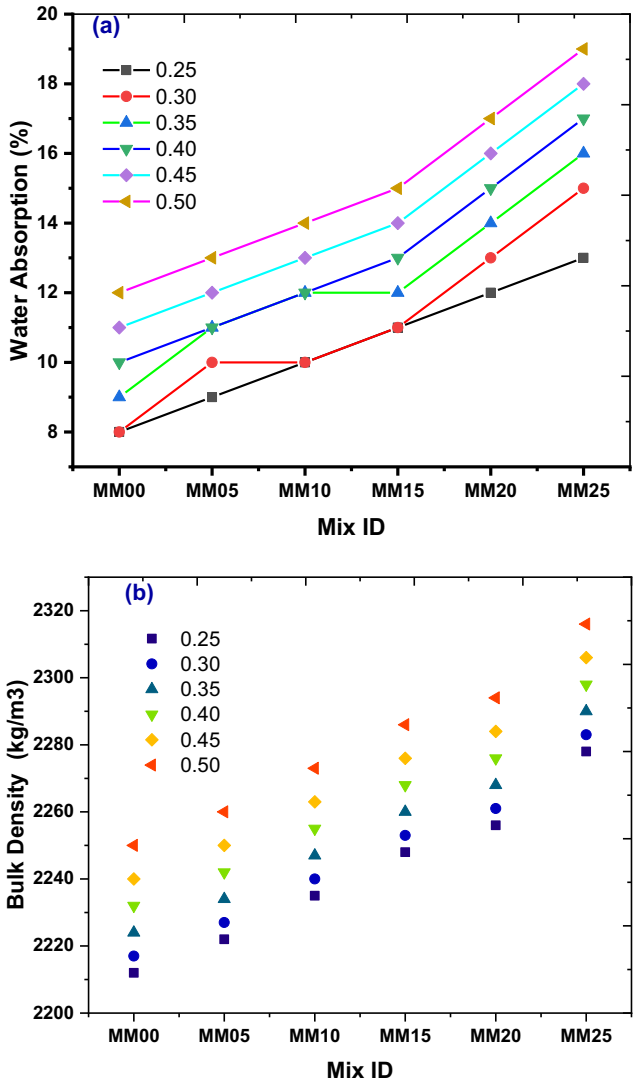

Fig. 13 – a. WA findings for various A/B ratios. b. BD findings for various A/B ratios.

and minimal BD was observed for MM00 at 2250 kg/m^3. The BD value observed for MM25 mix is 1.7%, 1.71%, 1.6%, 1.66%, 1.79%, and 1.8%,respectively, greater than MM00 mix. The BD value of MM25 with an A/B ratio of 0.50 is 1.66% higher than that of MM00.

Abundant silicon the MK and marble also consists of a certain extent of CaO. Reactive alumina led to react with the alkaline agent to produce geopolymer gel. While access of vibration carried out during making GPC results in bleeding of the geopolymer paste and brings gel upward [71,72]. Effect of aggregate inhibits gel from dissipating causing high gel content into the aggregate bottom. The presence of gel below aggregate leads to lower activator molarity and weaker alkalinity, and a slower rate polymerization, developing a binder with a porous structure. An increase in A/B ratio reduces the absorption property of GPC. The enhancement in PC properties is a cause of the increasing A/B ratio [73]. The increase in the A/B ratio increases the content of ~~Si~~ SiO_2because the activator contained KOH, which led to an enhancement in the SiO_2/Al_2O_3 in the matrix and made Si–O–Si bonds stronger [74].

3.8. *Elevated temperature resistance (ETR)*

For six different mix proportions, GPC was cast for A/B ranging from 0.25 to 0.50. Each specimen was heated in an elevated oven for 1 h at 200, 400, and 600 °C and then chilled to room temperature. The purpose of the test is to see how high temperatures affect GPC specimens and test the CS property. Fig. 14a shows the loss of CS for when GPC was exposed to 200 °C.

Cubes of 15 cm^3 were cast with an A/B ratio ranging from 0.25 to 0.50 to determine ETR. ETR value observed after experimentation ranging from 31 (minimum) to 61 (maximum) MPa for the A/B ratio of 0.25. The minimum and maximum ETR values were observed to be 34 and 54 MPa, respectively. The maximum ETR measured for MM00 was 54 MPa, and the minimum ETR measured for MM25 was 34 MPa. The lowest and highest ETR values for the A/B ratio of 0.30 were 37 and 61 MPa, respectively. Maximum ETR was measured at 61 MPa for the MM00 mix, while minimum ETR was measured at 37 MPa for the MM25 mix. The ETR value was observed from 32 to 50 MPa as the lowest and maximum value for the A/B ratio of 0.35. Maximum ETR was measured at 50 MPa for the MM00 mix, while minimum ETR was measured at 32 MPa for the MM25 mix. The lowest and highest ETR values for the A/B ratio of 0.40 were 29 and 48 MPa, respectively. The greatest ETR measured for MM00 was 48 MPa, and the minimum ETR measured for MM25 was 29 MPa. The lowest and highest ETR values for the A/B ratio of 0.45 were 25 and 43 MPa, respectively. The highest ETR for the MM00 mix was 43 MPa, while the lowest ETR for the MM25 mix was 25 MPa. The ETR value was recorded from 21 to 40 MPa as the lowest and maximum value for the A/B ratio of 0.50. The greatest ETR measured for MM00 was 47 MPa, and the minimum ETR measured for MM25 was 41 MPa.

Fig. 14b depicts the loss of CS when GPC was heated to 400 °C. After testing, ETR values ranged from 26 (minimum) to 58 (highest) MPa for 400 C, with A/B ratios ranging from 0.25 to 0.50. For A/B ratios of 0.25, the lowest and greatest ETR values were 33 and 58 MPa, respectively. Maximum ETR was measured at 58 MPa for the MM00 mix, while the minimum ETR was measured at 33 MPa for the MM25 mix. The lowest and highest ETR values for the A/B ratio of 0.30 were 30 and 53 MPa, respectively. The highest ETR for MM00 was measured to be 53 MPa, while the minimum ETR for MM25 was observed to be 30 MPa. The lowest and highest ETR values for the A/B ratio of 0.35 were 27 and 47 MPa, respectively. Maximum ETR was measured at 47 MPa for the MM00 mix, while minimum ETR was measured at 27 MPa for the MM25 mix. The lowest and highest ETR values for the A/B ratio of 0.40 were 25 and 43 MPa, respectively. The highest ETR for the MM00 mix was 43 MPa, while the lowest ETR for the MM25 mix was 25 MPa. The ETR value was observed from 21 to 40 MPa as the lowest and maximum value for the A/B ratio of 0.45. Maximum ETR was measured at 40 MPa for the MM00 mix, while minimum ETR was measured at 25 MPa for the MM25 mix. The ETR value was recorded from 18 to 33 MPa as the minimum and maximum value for the A/B ratio of 0.50.

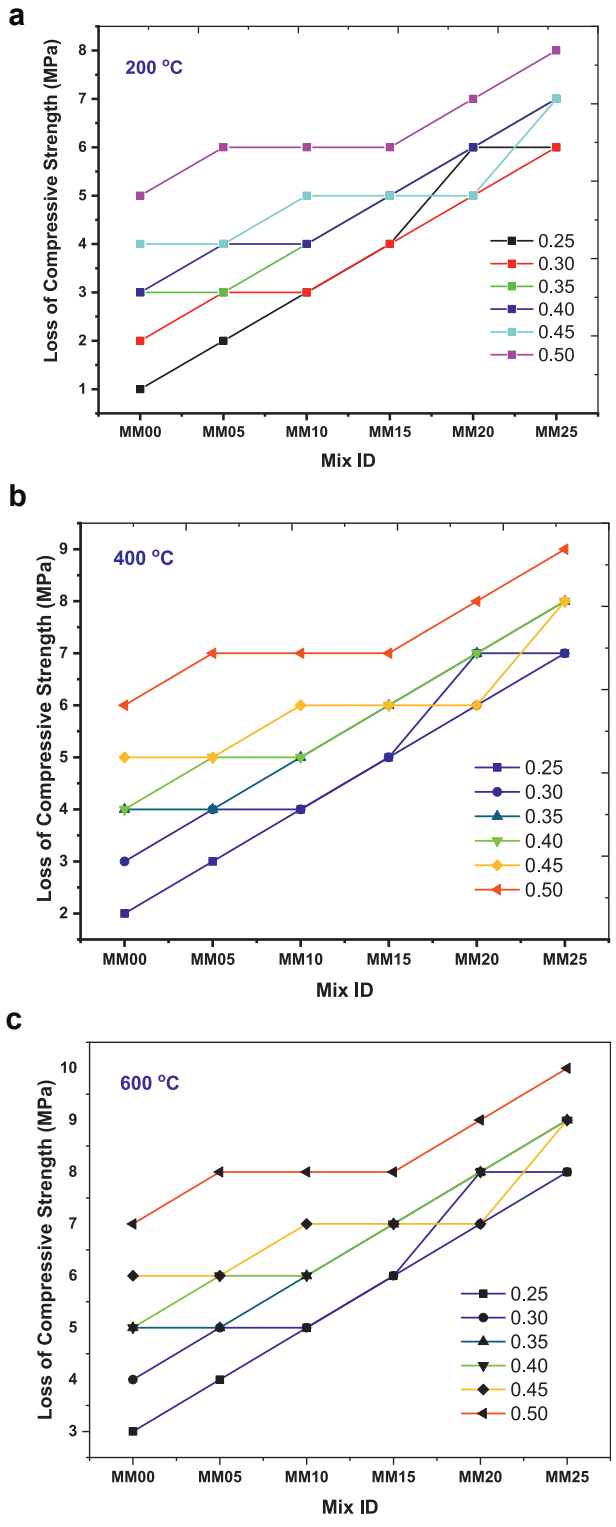

Fig. 14 – a. Loss of CS values for GPC cast for 200 °C compared for ambient curing. b. Loss of CS values for GPC cast for 400 °C compared for ambient curing. c. Loss of CS values for GPC cast for 600 °C compared for ambient curing.

Maximum ETR was measured at 33 MPa for the MM00 mix, while minimum ETR was measured at 18 MPa for the MM25 mix.

Fig. 14c depicts the loss of CS when GPC was heated to 600 °C. After testing, ETR values ranged from 24 (minimum) to 58 (highest) MPa for 600 C. With an A/B ratio of 0.25, the ETR value ranged from 28 to 53 MPa as the minimum and highest value. The highest ETR for MM00 was seen to be 53 MPa, while the minimum ETR for MM25 was reported to be 28 MPa. The lowest and highest ETR values for the A/B ratio of 0.30 were 27 and 52 MPa, respectively. The greatest ETR measured for MM00 was 52 MPa, and the minimum ETR measured for MM25 was 27 MPa. The lowest and highest ETR values for the A/B ratio of 0.35 were 25 and 43 MPa, respectively. The highest ETR for the MM00 mix was 43 MPa, while the lowest ETR for the MM25 mix was 25 MPa. The ETR value was recorded from 23 to 40 MPa as the minimum and maximum value for the A/B ratio of 0.40. Maximum ETR was measured at 40 MPa for the MM00 mix, while the minimum ETR was measured at 23 MPa for the MM25 mix. The lowest and highest ETR values for the A/B ratio of 0.45 were 20 and 37 MPa, respectively. Maximum ETR was measured at 37 MPa for the MM00 mix, while minimum ETR was measured at 20 MPa for the MM25 mix. The lowest and highest ETR values for the A/B ratio of 0.50 were 16 and 31 MPa, respectively. The greatest ETR measured for MM00 was 31 MPa, and the minimum ETR measured for MM25 was 16 MPa.

3.8.1. *Effect of elevated temperature on GPC*

According to the research findings, most research on the thermal performance of MK-based GPC has been limited to paste composites [75]. Because coarse aggregate accounts for a considerable portion of the volume of concrete, the ITZ has a significant impact on its behavior [76,77]. Furthermore, the thermal incompatibility of the aggregate and the GPC matrix influences the strength loss in concrete caused by exposure to high temperatures [78,79]. The literature study on binders is inadequate in several areas. As a result, the current work intends to close this gap by evaluating the behavior of MK-based GPC at ambient and increased temperatures of 200 °C, 400 °C, and 600 °C [29,71,80]. All visual observations for fresh and hardened specimens, CS development, STS, WA, and weight loss % due to exposure to elevated temperatures were evaluated [48,81]. The principal causes of strength loss after high temperatures are mass loss and thermal deformation caused by moisture evaporation. Water within the specimen, including both free and chemically bound water, flows to the outer surface and evaporates, producing internal microstructure damage and, as a result, strength degradation [24,82,83]. This process happens predominantly in the temperature range of 100–300 °C when water evaporation decreases, and hence the rate of strength deterioration decreases. At higher temperatures, the evaporation of chemically linked water continues. Although spalling due to pore pressure decreases at higher temperatures, the phase transition and composition change impact the residual strength of geopolymer [40,84,85]. Crack development between the aggregate and GPC matrix significantly impacts substantial strength loss, resulting in fractures and bond weakening at the aggregate–paste interface [31,69,86]. Since KOH has a more alkaline nature, its presence should cause raw materials containing aluminium silicate to dissolve and polymerize more readily, increasing CS. Additionally, it is claimed that KOH cations are better at zeolitizing in geopolymer-forming environments. This may be because they are smaller than sodium cations and can move more readily through the moist

gel network [20,87]. MK slurry samples were evaluated at KS/KH molar ratios ranging from 1.03 to 2 at temperatures ranging from 300 C to 600 C [8,88,89]. The residual CS dropped (for KS/KH 1.5) and then rose (for KS/KH > 1.5) at 300 C. It was proposed that the first reduction was caused by thermal shrinkage, which resulted in fracture development [19,90]. The growing tendency for specimens with KS/KH > 1.5, on the other hand, was related to matrix densification [91].

3.9. *Correlation and regression analysis between CS and STS in MK based GPC*

The relationship between CS and STS, from Australian standard AS3600, is given by equation

$$ft = 0.4\sqrt{fc} \tag{4}$$

$$\text{From, European code, CEB} - \text{FIP,} \quad ft = 0.3\, fc^{2/3} \tag{5}$$

$$\text{From, American Concrete Institute,} \quad ft = 0.59\sqrt{fc} \tag{6}$$

For the current work, the suggested empirical formula represented as

$$\text{Proposed empirical formula} \quad ft = 0.4801 \times fc^{0.5652} \tag{7}$$

where ft: STS,
fc:CS in MPa.

The values of Split Tensile strength value for experimental and results collected and calculated from various literature papers for different type codes are mentioned below in table.

It can be observed that, of the six equations tested, the predicted results determined from column (6) were the closest to the experimental ones. A regression analysis was utilized to show correlations between the tested further and projected findings to assess various STS values. Refer to Fig. 15 for the linearity value (R^2) derived from the proposed empirical formula findings. The data points presented in this graphic were gathered through GPC research. Examining these data reveals that the tensile strength values of GPC grew with the rise of compressive strength and remained virtually constant.

However, a previous study has demonstrated that GPC STS grew at a decreasing rate with incremental increases in CS. GPC's STS was proportionate to its CS multiplied by a special power. The association between the CS and STS of GPC, on the other hand, was linear (Fig. 11). The confidence intervals are calculated using the experimental data and Equation (7), and they represent the boundaries of the area where the accurate prediction between GPC ft and fc should be located with 96% certainty. The AS3600 model was the furthest away from the confidence and prediction intervals. This forecast continued to deviate from the actual points as its intensity increased. Only a tiny portion of the prediction lines generated by CEB-FIP and ACI 363 fell within the 95 and 97% confidence intervals. The relationship between CS and STS was found to vary linearly with R^2 value 0.98577 refer to Fig. 10b, Similarly for CS and FS, WA and BK, R^2 value is 0.98485, 0.96887 respectively refer to Fig. 10(c and d).

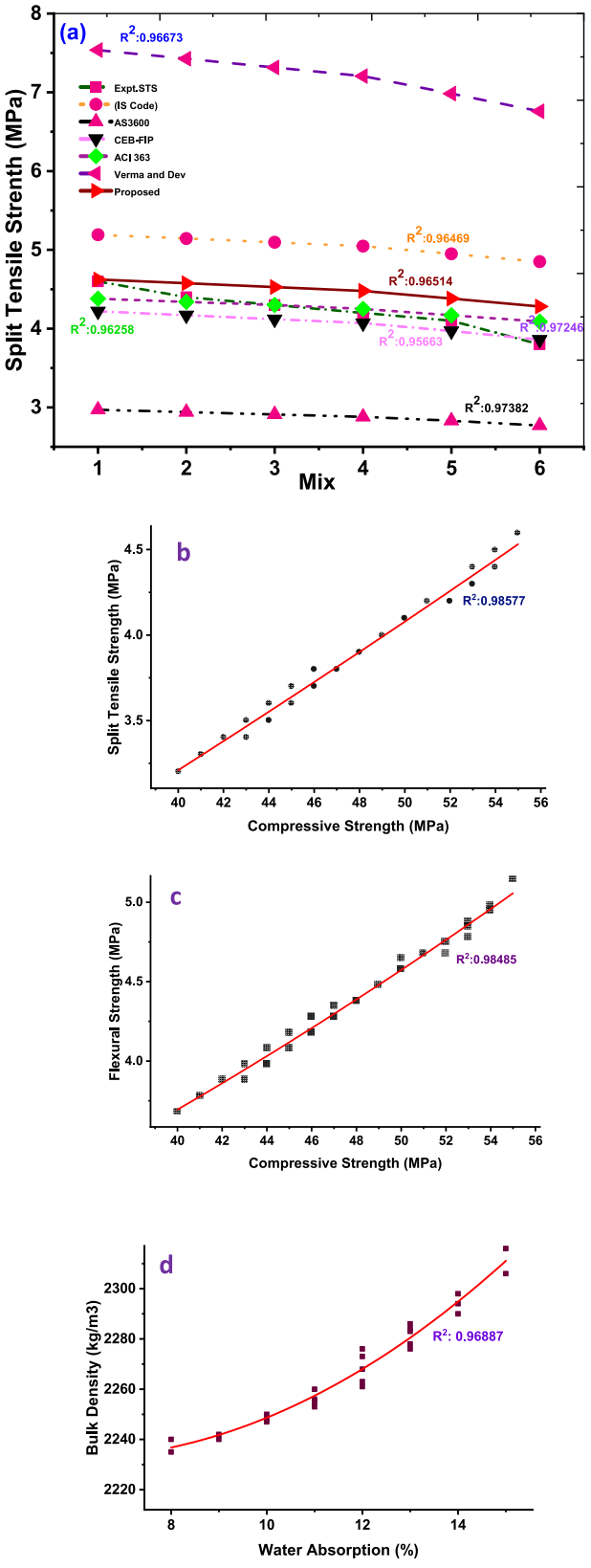

Fig. 15 – Regression analysis (a) for various STS values and proposed formula. (b) For CS v/s STS. (c) CS v/s FS. (d) WA v/s BK.

4. Conclusion

In present work Metakaolin based geopolymer concrete studied intensively, CS was lost at a faster rate for practically all mixtures when the temperature was raised from 200 °C to 600 °C; Although CS degraded as the exposure temperature increased. Even though several geopolymer mixes developed cracks, spalling, and corner breakage after being exposed to high temperatures, none of the mixes exhibited apparent cracks, spalling, or corner breakage. Since KOH is more alkaline, its inclusion ought to make raw materials containing aluminium silicate dissolve and polymerize more easily, enhancing CS. The potassium activator-based GPC demonstrates substantial strength properties as compared to ordinary concrete specimens. This is due to the interaction of aluminium silicate components with an alkaline solution, which provides GPC an excellent binding property and increases mechanical performances. During the curing process, the water in the liquids tended to escape from the sample bodies. It migrated towards the surfaces, causing tiny fractures to emerge due to the movement. The increased creation of microfractures was expected to boost the water absorption rates of the samples. Dissolution, N-A-S-H gel formation, and condensation are all steps in the geopolymerization process. At SiO_2/Al_2O_3 ratios less than 2:1, it was observed that soluble silicates accelerate metakaolin dissolution. When silicate is employed as an alkaline activator, Al_2O_3 dissolution becomes important in the creation of N-A-S-H gels, and large crystalline contents are generated at SiO_2/Al_2O_3 ratios less than 1:1.

Author contributions

Conceptualization, FAS and SVG; formal analysis, FAS; funding acquisition, SVG and KSN; investigation, FAS, SVG, and VBP,; resources, SVG, VBP; writing-original draft, FAS; writing-review and editing, FAS, SVG, VBP, and KSN. All authors have read and agreed to the published version of the manuscript.

Data availability statement

The data that support the findings of this study are available on request from the corresponding author [SVG].

Declaration of Competing Interest

The authors declare that they have no known competing financial interests or personal relationships that could have appeared to influence the work reported in this paper.

REFERENCES

[1] Garcia-Lodeiro I, Palomo A, Fernández-Jiménez A. 2 - an overview of the chemistry of alkali-activated cement-based binders. In: Pacheco-Torgal F, Labrincha JA, Leonelli C, Palomo A, Chindaprasirt P, editors. Handbook of alkali-activated cements, mortars and concretes. Oxford: Woodhead Publishing; 2015. p. 19–47. https://doi.org/10.1533/9781782422884.1.19.

[2] Khalifa AZ, Cizer Ö, Pontikes Y, Heath A, Patureau P, Bernal SA, et al. Advances in alkali-activation of clay minerals. Cement Concr Res 2020;132:106050. https://doi.org/10.1016/j.cemconres.2020.106050.

[3] Hassan A, Arif M, Shariq M. Age-dependent compressive strength and elastic modulus of fly ash-based geopolymer concrete. Struct Concr 2022;23:473–87. https://doi.org/10.1002/suco.202000372.

[4] Bakthavatchalam K, Rajendran M. An experimental investigation on potassium activator based geopolymer concrete incorporated with hybrid fibers. Mater Today Proc 2021;46:8494–501. https://doi.org/10.1016/j.matpr.2021.03.506.

[5] Mahmood A, Noman MT, Pechočiaková M, Amor N, Petrů M, Abdelkader M, et al. Geopolymers and fiber-reinforced concrete composites in civil engineering. Polymers 2021;13:2099. https://doi.org/10.3390/polym13132099.

[6] Ghannam S, Najm H, Vasconez R. Experimental study of concrete made with granite and iron powders as partial replacement of sand. Sustainable Materials and Technologies 2016;9:1–9. https://doi.org/10.1016/j.susmat.2016.06.001.

[7] Padmakar M, Barhmaiah B, Leela Priyanka M. Characteristic compressive strength of a geo polymer concrete. Mater Today Proc 2021;37:2219–22. https://doi.org/10.1016/j.matpr.2020.07.656.

[8] Das SK, Mishra J, Singh SK, Mustakim SM, Patel A, Das SK, et al. Characterization and utilization of rice husk ash (RHA) in fly ash – blast furnace slag based geopolymer concrete for sustainable future. Mater Today Proc 2020;33:5162–7. https://doi.org/10.1016/j.matpr.2020.02.870.

[9] Lee WKW, van Deventer JSJ. Chemical interactions between siliceous aggregates and low-Ca alkali-activated cements. Cement Concr Res 2007;37:844–55. https://doi.org/10.1016/j.cemconres.2007.03.012.

[10] Amran YHM, Alyousef R, Alabduljabbar H, El-Zeadani M. Clean production and properties of geopolymer concrete; A review. J Clean Prod 2020;251:119679. https://doi.org/10.1016/j.jclepro.2019.119679.

[11] Chindaprasirt P, Jaturapitakkul C, Chalee W, Rattanasak U. Comparative study on the characteristics of fly ash and bottom ash geopolymers. Waste Manag 2009;29:539–43. https://doi.org/10.1016/j.wasman.2008.06.023.

[12] Shilar FA, Ganachari SV, Patil VB, Nisar KS, Abdel-Aty A-H, Yahia IS. Evaluation of the effect of granite waste powder by varying the molarity of activator on the mechanical properties of ground granulated blast-furnace slag-based geopolymer concrete. Polymers 2022;14:306. https://doi.org/10.3390/polym14020306.

[13] Shilar FA, Ganachari SV, Patil VB, Khan TMY, Dawood Abdul Khadar S. Molarity activity effect on mechanical and microstructure properties of geopolymer concrete: a review. Case Stud Constr Mater 2022;16:e01014. https://doi.org/10.1016/j.cscm.2022.e01014.

[14] Garcia-Lodeiro I, Palomo A, Fernández-Jiménez A, Macphee DE. Compatibility studies between N-A-S-H and C-A-S-H gels. Study in the ternary diagram Na2O–CaO–Al2O3–SiO2–H2O. Cement Concr Res 2011;41:923–31. https://doi.org/10.1016/j.cemconres.2011.05.006.

[15] Al-Majidi MH, Lampropoulos A, Cundy A, Meikle S. Development of geopolymer mortar under ambient temperature for in situ applications. Construct Build Mater 2016;120:198–211. https://doi.org/10.1016/j.conbuildmat.2016.05.085.

[16] Meesala CR, Verma NK, Kumar S. Critical review on fly-ash based geopolymer concrete. Struct Concr 2020;21:1013–28. https://doi.org/10.1002/suco.201900326.
[17] Huiskes DMA, Keulen A, Yu QL, Brouwers HJH. Design and performance evaluation of ultra-lightweight geopolymer concrete. Mater Des 2016;89:516–26. https://doi.org/10.1016/j.matdes.2015.09.167.
[18] Ganesh AC, Muthukannan M. Development of high performance sustainable optimized fiber reinforced geopolymer concrete and prediction of compressive strength. J Clean Prod 2021;282:124543. https://doi.org/10.1016/j.jclepro.2020.124543.
[19] Luhar S, Chaudhary S, Luhar I. Development of rubberized geopolymer concrete: strength and durability studies. Construct Build Mater 2019;204:740–53. https://doi.org/10.1016/j.conbuildmat.2019.01.185.
[20] Nikoloutsopoulos N, Sotiropoulou A, Kakali G, Tsivilis S. Physical and mechanical properties of fly ash based geopolymer concrete compared to conventional concrete. Buildings 2021;11:178. https://doi.org/10.3390/buildings11050178.
[21] Zhang P, Wang K, Wang J, Guo J, Ling Y. Macroscopic and microscopic analyses on mechanical performance of metakaolin/fly ash based geopolymer mortar. J Clean Prod 2021;294:126193. https://doi.org/10.1016/j.jclepro.2021.126193.
[22] Rashidian-Dezfouli H, Rangaraju PR. Study on the effect of selected parameters on the alkali-silica reaction of aggregate in ground glass fiber and fly ash-based geopolymer mortars. Construct Build Mater 2021;271:121549. https://doi.org/10.1016/j.conbuildmat.2020.121549.
[23] Sethi H, Bansal PP, Sharma R. Effect of addition of GGBS and glass powder on the properties of geopolymer concrete. Iran J Sci Technol Trans Civ Eng 2019;43:607–17. https://doi.org/10.1007/s40996-018-0202-4.
[24] Lloyd RR, Provis JL, van Deventer JSJ. Pore solution composition and alkali diffusion in inorganic polymer cement. Cement Concr Res 2010;40:1386–92. https://doi.org/10.1016/j.cemconres.2010.04.008.
[25] Singh SB, Munjal P. Bond strength and compressive stress-strain characteristics of brick masonry. J Build Eng 2017;9:10–6. https://doi.org/10.1016/j.jobe.2016.11.006.
[26] Lo K-W, Lin K-L, Cheng T-W, Chang Y-M, Lan J-Y. Effect of nano-SiO2 on the alkali-activated characteristics of spent catalyst metakaolin-based geopolymers. Construct Build Mater 2017;143:455–63. https://doi.org/10.1016/j.conbuildmat.2017.03.152.
[27] Chithambaram SJ, Kumar S, Prasad MM, Adak D. Effect of parameters on the compressive strength of fly ash based geopolymer concrete. Struct Concr 2018;19:1202–9. https://doi.org/10.1002/suco.201700235.
[28] Boca Santa RAA, Soares C, Riella HG. Geopolymers with a high percentage of bottom ash for solidification/immobilization of different toxic metals. J Hazard Mater 2016;318:145–53. https://doi.org/10.1016/j.jhazmat.2016.06.059.
[29] Albidah A, Alqarni AS, Abbas H, Almusallam T, Al-Salloum Y. Behavior of Metakaolin-Based geopolymer concrete at ambient and elevated temperatures. Construct Build Mater 2022;317:125910. https://doi.org/10.1016/j.conbuildmat.2021.125910.
[30] Chindaprasirt P, Chalee W. Effect of sodium hydroxide concentration on chloride penetration and steel corrosion of fly ash-based geopolymer concrete under marine site. Construct Build Mater 2014;63:303–10. https://doi.org/10.1016/j.conbuildmat.2014.04.010.
[31] Krishna Rao A, Kumar DR. Effect of various alkaline binder ratio on geopolymer concrete under ambient curing condition. Mater Today Proc 2020;27:1768–73. https://doi.org/10.1016/j.matpr.2020.03.682.
[32] Aliabdo AA, Abd Elmoaty AEM, Salem HA. Effect of water addition, plasticizer and alkaline solution constitution on fly ash based geopolymer concrete performance. Construct Build Mater 2016;121:694–703. https://doi.org/10.1016/j.conbuildmat.2016.06.062.
[33] Ravikumar D, Neithalath N. Effects of activator characteristics on the reaction product formation in slag binders activated using alkali silicate powder and NaOH. Cement Concr Compos 2012;34:809–18. https://doi.org/10.1016/j.cemconcomp.2012.03.006.
[34] IS 1199. Methods of sampling and analysis of concrete. 1959. p. 49.
[35] Malkawi AB, Nuruddin MF, Fauzi A, Almattarneh H, Mohammed BS. Effects of alkaline solution on properties of the HCFA geopolymer mortars. Procedia Eng 2016;148:710–7. https://doi.org/10.1016/j.proeng.2016.06.581.
[36] Mousavinejad SHG, Gashti MF. Effects of alkaline solution/binder and Na2SiO3/NaOH ratios on fracture properties and ductility of ambient-cured GGBFS based heavyweight geopolymer concrete. Structures 2021;32:2118–29. https://doi.org/10.1016/j.istruc.2021.04.008.
[37] Hanjitsuwan S, Hunpratub S, Thongbai P, Maensiri S, Sata V, Chindaprasirt P. Effects of NaOH concentrations on physical and electrical properties of high calcium fly ash geopolymer paste. Cement Concr Compos 2014;45:9–14. https://doi.org/10.1016/j.cemconcomp.2013.09.012.
[38] EL Alouani M, Alehyen S, EL Achouri M, Hajjaji A, Ennawaoui C, Taibi M. Influence of the nature and rate of alkaline activator on the physicochemical properties of fly ash-based geopolymers. Adv Civ Eng 2020;2020:e8880906. https://doi.org/10.1155/2020/8880906.
[39] Álvarez-Ayuso E, Querol X, Plana F, Alastuey A, Moreno N, Izquierdo M, et al. Environmental, physical and structural characterisation of geopolymer matrixes synthesised from coal (co-)combustion fly ashes. J Hazard Mater 2008;154:175–83. https://doi.org/10.1016/j.jhazmat.2007.10.008.
[40] Gutiérrez RM, Villaquirán-Caicedo M, Ramírez-Benavides S, Astudillo M, Mejía D. Evaluation of the antibacterial activity of a geopolymer mortar based on metakaolin supplemented with TiO2 and CuO particles using glass waste as fine aggregate. Coatings 2020;10:157. https://doi.org/10.3390/coatings10020157.
[41] John SK, Nadir Y, Girija K. Effect of source materials, additives on the mechanical properties and durability of fly ash and fly ash-slag geopolymer mortar: a review. Construct Build Mater 2021;280:122443. https://doi.org/10.1016/j.conbuildmat.2021.122443.
[42] IS 516. Method of tests for strength of concrete. 1959. p. 30.
[43] Perez-Cortes P, Escalante-Garcia JI. Gel composition and molecular structure of alkali-activated metakaolin-limestone cements. Cement Concr Res 2020;137:106211. https://doi.org/10.1016/j.cemconres.2020.106211.
[44] Raijiwala DB, Patil HS. Geopolymer concrete A green concrete. 2010 2nd international conference on chemical, biological and environmental engineering. 2010. p. 202–6. https://doi.org/10.1109/ICBEE.2010.5649609.
[45] Singh B, Ishwarya G, Gupta M, Bhattacharyya SK. Geopolymer concrete: a review of some recent developments. Construct Build Mater 2015;85:78–90. https://doi.org/10.1016/j.conbuildmat.2015.03.036.
[46] Charkhtab Moghaddam S, Madandoust R, Jamshidi M, Nikbin IM. Mechanical properties of fly ash-based geopolymer concrete with crumb rubber and steel fiber under ambient and sulfuric acid conditions. Construct Build Mater 2021;281:122571. https://doi.org/10.1016/j.conbuildmat.2021.122571.

[47] Jayarajan G, Arivalagan S. An experimental studies of geopolymer concrete incorporated with fly-ash & GGBS. Mater Today Proc 2021;45:6915–20. https://doi.org/10.1016/j.matpr.2021.01.285.
[48] Mishra J, Das SK, Krishna R, Nanda B, Patro S, Mustakim S. Synthesis and characterization of a new class of geopolymer binder utilizing ferrochrome ash (FCA) for sustainable industrial waste management. 2020. https://doi.org/10.1016/j.matpr.2020.02.832.
[49] Ganachari SV. Polymers for energy applications. In: Martínez LMT, Kharissova OV, Kharisov BI, editors. Handbook of ecomaterials. Cham: Springer International Publishing; 2019. p. 3011–27. https://doi.org/10.1007/978-3-319-68255-6_194.
[50] Hallad SA, Banapurmath NR, Khan TMY, Umarfarooq MA, Soudagar MEM, Hunashyal AM, et al. Statistical analysis of polymer nanocomposites for mechanical properties. Molecules 2021;26:4135. https://doi.org/10.3390/molecules26144135.
[51] Oyebisi S, Ede A, Olutoge F, Omole D. Geopolymer concrete incorporating agro-industrial wastes: effects on mechanical properties, microstructural behaviour and mineralogical phases. Construct Build Mater 2020;256:119390. https://doi.org/10.1016/j.conbuildmat.2020.119390.
[52] IS 5816. Method of test splitting tensile strength of concrete. 1999. p. 14.
[53] Hallad SA, Banapurmath NR, Bhadrakali AS, Patil AY, Hunashyal AM, Ganachari SV, et al. Nanoceramic composites for nuclear radiation attenuation. Materials 2022;15:262. https://doi.org/10.3390/ma15010262.
[54] Amran M, Al-Fakih A, Chu SH, Fediuk R, Haruna S, Azevedo A, et al. Long-term durability properties of geopolymer concrete: an in-depth review. Case Stud Constr Mater 2021;15. https://doi.org/10.1016/j.cscm.2021.e00661.
[55] Amran M, Al-Fakih A, Chu SH, Fediuk R, Haruna S, Azevedo A, et al. Long-term durability properties of geopolymer concrete: an in-depth review. Case Stud Constr Mater 2021;15:e00661. https://doi.org/10.1016/j.cscm.2021.e00661.
[56] de Azevedo ARG, Marvila MT, de Oliveira LB, Ferreira WM, Colorado H, Teixeira SR, et al. Circular economy and durability in geopolymers ceramics pieces obtained from glass polishing waste. Int J Appl Ceram Technol 2021:18. https://doi.org/10.1111/ijac.13780.
[57] Marvila MT, De Azevedo ARG, De Matos PR, Monteiro SN, Vieira CMF. Materials for production of high and ultra-high performance concrete: review and perspective of possible novel materials. Mater 2021;14. https://doi.org/10.3390/ma14154304.
[58] Ghafoor MT, Khan QS, Qazi AU, Sheikh MN, Hadi MNS. Influence of alkaline activators on the mechanical properties of fly ash based geopolymer concrete cured at ambient temperature. Construct Build Mater 2021;273:121752. https://doi.org/10.1016/j.conbuildmat.2020.121752.
[59] Lee NK, Lee HK. Influence of the slag content on the chloride and sulfuric acid resistances of alkali-activated fly ash/slag paste. Cement Concr Compos 2016;72:168–79. https://doi.org/10.1016/j.cemconcomp.2016.06.004.
[60] Shi H, Ma H, Tian L, Yang J, Yuan J. Effect of microwave curing on metakaolin-quartz-based geopolymer bricks. Construct Build Mater 2020;258:120354. https://doi.org/10.1016/j.conbuildmat.2020.120354.
[61] Shilar FA, Ganachari SV, Patil VB. Investigation of the effect of granite waste powder as a binder for different molarity of geopolymer concrete on fresh and mechanical properties. Mater Lett 2021:131302. https://doi.org/10.1016/j.matlet.2021.131302.
[62] Shi X, Zhang C, Wang X, Zhang T, Wang Q. Response surface methodology for multi-objective optimization of fly ash-GGBS based geopolymer mortar. Construct Build Mater 2021:125644. https://doi.org/10.1016/j.conbuildmat.2021.125644.
[63] He PY, Zhang YJ, Chen H, Liu LC. Development of an eco-efficient CaMoO4/electroconductive geopolymer composite for recycling silicomanganese slag and degradation of dye wastewater. J Clean Prod 2019;208:1476–87. https://doi.org/10.1016/j.jclepro.2018.10.176.
[64] Pilehvar S, Cao VD, Szczotok AM, Valentini L, Salvioni D, Magistri M, et al. Mechanical properties and microscale changes of geopolymer concrete and Portland cement concrete containing micro-encapsulated phase change materials. Cement Concr Res 2017;100:341–9. https://doi.org/10.1016/j.cemconres.2017.07.012.
[65] Cai J, Pan J, Han J, Lin Y, Sheng Z. Impact behaviours of engineered geopolymer composite exposed to elevated temperatures. Construct Build Mater 2021;312:125421. https://doi.org/10.1016/j.conbuildmat.2021.125421.
[66] Ondova M, Estokova A. Environmental impact assessment of building foundation in masonry family houses related to the total used building materials. Environ Prog Sustain Energy 2016;35:1113–20. https://doi.org/10.1002/ep.12307.
[67] Okoye FN, Durgaprasad J, Singh NB. Mechanical properties of alkali activated flyash/Kaolin based geopolymer concrete. Construct Build Mater 2015;98:685–91. https://doi.org/10.1016/j.conbuildmat.2015.08.009.
[68] Shehab HK, Eisa AS, Wahba AM. Mechanical properties of fly ash based geopolymer concrete with full and partial cement replacement. Construct Build Mater 2016;126:560–5. https://doi.org/10.1016/j.conbuildmat.2016.09.059.
[69] Moya JS, Cabal B, Sanz J, Torrecillas R. Metakaolin-nanosilver as biocide agent in geopolymer. Developments in strategic materials and computational design III. John Wiley & Sons; 2012. p. 1–11. https://doi.org/10.1002/9781118217542.ch1.
[70] ASTM C1585-20 n.d. https://www.techstreet.com/standards/astm-c1585-20?product_id=2189851 (accessed December 26, 2021).
[71] Duxson P, Provis JL, Lukey GC, van Deventer JSJ. The role of inorganic polymer technology in the development of 'green concrete. Cement Concr Res 2007;37:1590–7. https://doi.org/10.1016/j.cemconres.2007.08.018.
[72] Ismail I, Bernal SA, Provis JL, San Nicolas R, Hamdan S, van Deventer JSJ. Modification of phase evolution in alkali-activated blast furnace slag by the incorporation of fly ash. Cement Concr Compos 2014;45:125–35. https://doi.org/10.1016/j.cemconcomp.2013.09.006.
[73] Liew Y-M, Heah C-Y, Li L, Jaya NA, Abdullah MMAB, Tan SJ, et al. Formation of one-part-mixing geopolymers and geopolymer ceramics from geopolymer powder. Construct Build Mater 2017;156:9–18. https://doi.org/10.1016/j.conbuildmat.2017.08.110.
[74] Al Bakri Abdullah MM, Kamarudin H, Abdulkareem OAKA, Ghazali CMR, Rafiza AR, Norazian MN. Optimization of alkaline activator/fly ASH ratio on the compressive strength of manufacturing fly ASH-BASED geopolymer. Appl Mech Mater 2012;110–116:734–9. https://doi.org/10.4028/www.scientific.net/AMM.110-116.734.
[75] Luo Z, Li W, Wang K, Castel A, Shah SP. Comparison on the properties of ITZs in fly ash-based geopolymer and Portland cement concretes with equivalent flowability. Cement Concr Res 2021;143:106392. https://doi.org/10.1016/j.cemconres.2021.106392.
[76] Vora PR, Dave UV. Parametric studies on compressive strength of geopolymer concrete. Procedia Eng 2013;51:210–9. https://doi.org/10.1016/j.proeng.2013.01.030.
[77] Sarkar M, Dana K. Partial replacement of metakaolin with red ceramic waste in geopolymer. Ceram Int 2021;47:3473–83. https://doi.org/10.1016/j.ceramint.2020.09.191.

[78] Aly AM, El-Feky MS, Kohail M, Nasr E-SAR. Performance of geopolymer concrete containing recycled rubber. Construct Build Mater 2019;207:136–44. https://doi.org/10.1016/j.conbuildmat.2019.02.121.
[79] Saloni, Parveen, Pham TM, Lim YY, Pradhan SS, Jatin, et al. Performance of rice husk Ash-Based sustainable geopolymer concrete with Ultra-Fine slag and Corn cob ash. Construct Build Mater 2021;279:122526. https://doi.org/10.1016/j.conbuildmat.2021.122526.
[80] Yeoh MLY, Ukritnukun S, Rawal A, Davies J, Kang BJ, Burrough K, et al. Mechanistic impacts of long-term gamma irradiation on physicochemical, structural, and mechanical stabilities of radiation-responsive geopolymer pastes. J Hazard Mater 2021;407:124805. https://doi.org/10.1016/j.jhazmat.2020.124805.
[81] Ryu GS, Lee YB, Koh KT, Chung YS. The mechanical properties of fly ash-based geopolymer concrete with alkaline activators. Construct Build Mater 2013;47:409–18. https://doi.org/10.1016/j.conbuildmat.2013.05.069.
[82] Zerzouri M, Bouchenafa O, Hamzaoui R, Ziyani L, Alehyen S. Physico-chemical and mechanical properties of fly ash based-geopolymer pastes produced from pre-geopolymer powders obtained by mechanosynthesis. Construct Build Mater 2021;288:123135. https://doi.org/10.1016/j.conbuildmat.2021.123135.
[83] Medri V, Papa E, Mazzocchi M, Laghi L, Morganti M, Francisconi J, et al. Production and characterization of lightweight vermiculite/geopolymer-based panels. Mater Des 2015;85:266–74. https://doi.org/10.1016/j.matdes.2015.06.145.
[84] Abeysundara UGY, Babel S. A quest for sustainable materials for building elements in Sri Lanka: Foundations. Environ Prog Sustain Energy 2010;29:370–81. https://doi.org/10.1002/ep.10420.
[85] Al-Qutaifi S, Nazari A, Bagheri A. Mechanical properties of layered geopolymer structures applicable in concrete 3D-printing. Construct Build Mater 2018;176:690–9. https://doi.org/10.1016/j.conbuildmat.2018.04.195.
[86] Qin Y, Chen X, Li B, Guo Y, Niu Z, Xia T, et al. Study on the mechanical properties and microstructure of chitosan reinforced metakaolin-based geopolymer. Construct Build Mater 2021;271:121522. https://doi.org/10.1016/j.conbuildmat.2020.121522.
[87] Saloni Parveen, Yan Lim Y, Pham TM. Influence of Portland cement on performance of fine rice husk ash geopolymer concrete: strength and permeability properties. Construct Build Mater 2021;300:124321. https://doi.org/10.1016/j.conbuildmat.2021.124321.
[88] Elyamany HE, Abd Elmoaty AEM, Elshaboury AM. Setting time and 7-day strength of geopolymer mortar with various binders. Construct Build Mater 2018;187:974–83. https://doi.org/10.1016/j.conbuildmat.2018.08.025.
[89] Das SK, Shrivastava S. Siliceous fly ash and blast furnace slag based geopolymer concrete under ambient temperature curing condition. Struct Concr 2021;22:E341–51. https://doi.org/10.1002/suco.201900201.
[90] Ma C-K, Awang AZ, Omar W. Structural and material performance of geopolymer concrete: a review. Construct Build Mater 2018;186:90–102. https://doi.org/10.1016/j.conbuildmat.2018.07.111.
[91] Nie Q, Hu W, Huang B, Shu X, He Q. Synergistic utilization of red mud for flue-gas desulfurization and fly ash-based geopolymer preparation. J Hazard Mater 2019;369:503–11. https://doi.org/10.1016/j.jhazmat.2019.02.059.
[92] Verma M, Dev N. Sodium hydroxide effect on the mechanical properties of flyash-slag based geopolymer concrete. Struct Concr 2021;22:E368–79. https://doi.org/10.1002/suco.202000068.
[93] Jayarajan G, Arivalagan S. An experimental studies of geopolymer concrete incorporated with fly-ash & GGBS. Mater Today Proc 2021;45(7):6915–20. https://doi.org/10.1016/j.matpr.2021.01.285.